Gravitational waves from coalescing binaries: Detection strategies and Monte Carlo estimation of parameters

R. Balasubramanian, B. S. Sathyaprakash,* and S. V. Dhurandhar
Inter-University Centre for Astronomy and Astrophysics, Post Bag 4, Ganeshkhind, Pune 411 007, India
(Received 4 August 1995)

The detection of gravitational waves from astrophysical sources is probably one of the most keenly awaited events in the history of astrophysics. The paucity of gravitational wave sources and the relative difficulty in detecting such waves, as compared to those in the electromagnetic domain, necessitate the development of optimal data analysis techniques to detect the signal, as well as to extract the maximum possible information from the detected signals. Coalescing binary systems are one of the most promising sources of gravitational waves. This is due to the fact that such sources are easier to model and thus one can design detection strategies particularly tuned to such signals. A lot of attention has been devoted in the literature to studying such techniques and most of the work has revolved around the Weiner filtering and the maximum likelihood estimators of the parameters of the binary system. We investigate such techniques with the aid of differential geometry which provides geometric insight into the problem. Such a formalism allows us to explore the merits and faults of a detection scheme independent of the parameters chosen to represent the waveform. The formalism also generalizes the problem of choosing an optimal set of templates to detect a known waveform buried in noisy data. We stress the need for finding a set of *convenient* parameters for the waveform and show that even after the inclusion of the second-order post-Newtonian corrections, the waveform can essentially be detected by employing a one-dimensional lattice of templates. This would be very useful both for the purpose of carrying out the simulations as well as for the actual detection process. After setting up such a formalism we carry out a Monte Carlo simulation of the detection process for the initial LIGO-VIRGO configuration for the first post-Newtonian corrected coalescing binary waveform. We compare the results of our simulations with the currently available estimates of the accuracies in the determination of the parameters and the probability distribution of the maximum likelihood estimators. Our results suggest that the covariance matrix underestimates, by over a factor of 2, the actual errors in the estimation of parameters even when the signal-to-noise ratio is as high as 10. As only a tiny fraction of the events is expected to be detected with a signal-to-noise higher than this value, the covariance matrix is grossly inadequate to describe the errors in the measurement of the parameters of the waveform. It is found from our Monte Carlo simulations that the deviations from the covariance matrix are more in the case of the first post-Newtonian waveform than in the case of the Newtonian one. Inclusion of higher-order post-Newtonian corrections introduces new parameters that are correlated with those at the lower post-Newtonian waveform. Such correlations are expected to further increase the discrepancy of the covariance matrix results with those inferred from Monte Carlo simulations. Consequently, numerical simulations that take into account post-Newtonian corrections beyond the first post-Newtonian order are needed in order to get a clearer picture about the accuracy in the determination of parameters. We find that with the aid of the instant of coalescence the direction to the source can be determined more accurately than with the time of arrival.

PACS number(s): 04.30.Db, 04.80.Nn, 95.85.Sz, 97.80.Af

I. INTRODUCTION

Laser interferometric detectors of gravitational waves such as the Laser Interferometric Gravitational Wave Observatory (LIGO) [1] and VIRGO [2] are expected to be operational by the turn of the century. Gravitational waves from coalescing binary systems of black holes and neutron stars are relatively "clean" waveforms in the sense that they are easier to model and for this reason they are among the most important candidate sources for interferometric detectors. Binary systems are also valuable sources of astrophysical information as one can probe the universe up to cosmological distances. For instance, statistical analysis of several binary coalescences enables the estimation of the Hubble constant to an accuracy better than 10% [3,4]. Events that produce a high signal-to-noise ratio (SNR) can be potentially used to observe such nonlinear effects as gravitational wave tails

*Present address: Department of Physics and Astronomy, University of Wales, Cardiff, Wales.

and to put general relativity to the test in the strongly nonlinear regime [5]. Because of the weak coupling of gravitational radiation with matter, the signal waveform has a very low amplitude and will not stand above the detector noise. In addition to the ongoing efforts to reduce the noise, and hence increase the sensitivity of the detector, a considerable amount of research activity has gone into the development of efficient and robust data analysis techniques to extract signals buried in very noisy data. For a recent review on gravitational waves from compact objects and their detection see Thorne [6,7].

Various data analysis schemes have been suggested for the detection of the "chirp" waveform from such systems [8–10]. Among them the technique of Weiner filtering is the most promising [10–12]. Briefly, this technique involves correlating the detector output with a set of templates, each of which is tuned to detect the signal with a particular set of parameters. This requires the signal to be known to a high level of accuracy. The fully general relativistic waveform from a coalescing binary system of stars is as yet unavailable. In the absence of such an exact solution, there have been efforts to find solutions perturbatively. Most of the work done in this area aims at computing the waveform correct to a high degree of accuracy so that theoretical templates computed based on them will obtain close to the optimal value of the SNR possible, when correlated with the detector output if the corresponding signal is present. In general, the number of parameters increases as we incorporate the higher order corrections. It is clear that the number of templates depends upon the number of signal parameters. As a consequence, the computing power for an on-line analysis will be greater for a larger number of parameters. In view of this restriction in computing power it is necessary to choose the templates in an optimal manner. This paper in part deals with this question. Investigations until now have been restricted to either choosing a finite subset of the signal space as templates [13,14] or choosing templates from the "Newtonian" or the "first post-Newtonian" family of waveforms [15–18]. We generalize this problem by using the language of differential geometry. We show that it is unnecessary to restrict oneself to templates that are matched exactly to any particular signal.

Differential geometry has been used in statistics before (see [19] and references therein) and the standard approach is to treat a set of parametrized probability distributions corresponding to a particular statistical model as a manifold. The parameters of the distribution serve as coordinates on this manifold. In statistical theory one frequently comes across the Fisher information matrix whose inverse gives a lower bound for the errors in the estimation of the parameters of a distribution. The Fisher information matrix turns out to be a very natural metric on the manifold of probability distributions and this metric can be used profitably in understanding the properties of a particular statistical model. Though differential geometric language has been used in the literature pertaining to gravitational wave data analysis [20] the techniques of differential geometry have not been made use of in the design of efficient search templates, estimation of parameters, etc. See however [21]. Here in our paper we treat the set of coalescing binary signals corresponding to various parameters of the binary as a submanifold in the linear space of all detector outputs. We show in this paper that both the above-mentioned manifolds are equivalent as far as their metrical properties are concerned. The geometric approach turns out to be useful not only in clarifying various aspects of signal analysis but also helps us to pose the question of optimal detection in a more general setting.

Once a signal has been detected we can estimate the parameters of the binary. We assume that the parameters of the signal are the same as those of the template with which the maximum correlation is obtained. The errors involved in such an estimation have been worked out by several authors [5,18,20,22–28], for the case of a "high" SNR and for the Newtonian and post-Newtonian waveforms using a single and a network of detectors. For the case of low SNR's one has to resort to numerical simulations. We have started a project to carry out exhaustive numerical simulations specifically designed to compute the errors in the estimation of parameters and covariances among them at various post-Newtonian orders, for circular and eccentric orbits, with and without spin effects, and for different optical configurations of the interferometer. In this paper we report the results for the case of the initial LIGO configuration, taking into account only the first post-Newtonian corrections and assuming circular orbits. Going beyond this requires a tremendous amount of computing power which is just becoming available.

The rest of the paper is organized as follows. In Sec. II we describe the waveform from a coalescing binary system at various post-Newtonian orders. We introduce, following [29], a set of parameters called "chirp times." These parameters are found to be very convenient when we carry out Monte Carlo simulations. It turns out that the covariance matrix is independent of these parameters and hence it is sufficient to carry out the simulations only for a particular set of parameters. In Sec. III we develop a geometric interpretation of the signal analysis. We begin by introducing a metric on the manifold from a scalar product, which comes naturally from the theory of matched filtering, and then show that this metric is the same as the one used by Amari [19]. Using the geometric approach we address the question of optimal filter placement and show that for the purpose of detection it is optimal to choose templates outside the signal manifold. The covariance matrix of errors and covariances is shown to be the inverse of the metric on the manifold. In Sec. IV we discuss the results of our simulations and compare the numerically obtained values and those suggested by the covariance matrix. We find substantial discrepancies in the predictions of the two methods. It is believed that the coalescing binary waveform shuts off abruptly at the onset of the plunge orbit. This has a major effect on the computations of the covariance matrix [20] as well as on the Monte Carlo simulations. We discuss the effects of higher post-Newtonian corrections to the waveform. We also emphasisize the use of the instant of coalescence as a parameter in order to determine the direction to the

source rather than the time of arrival [30]. Finally in Sec. V we summarize our results and indicate future directions.

II. COALESCING BINARY WAVEFORMS

For the purpose of constructing templates for on-line detection, it is sufficient to work with the so called *restricted* post-Newtonian gravitational waveform. In this approximation the post-Newtonian corrections are incorporated only in the phase of the waveform, while ignoring corresponding corrections to the amplitude [31]. Consequently, the restricted post-Newtonian waveforms only contain the dominant frequency equal to twice the orbital frequency of the binary computed up to the relevant order. In the restricted post-Newtonian approximation the gravitational waves from a binary system of stars, modeled as point masses orbiting about each other in a circular orbit, induce a strain $h(t)$ at the detector given by

$$h(t) = A[\pi f(t)]^{2/3} \cos[\varphi(t)], \tag{2.1}$$

where $f(t)$ is the instantaneous gravitational wave frequency, the constant A involves the distance to the binary, its reduced and total mass, and the antenna pattern of the detector [10], and the phase of the waveform $\varphi(t)$ contains several pieces corresponding to different post-Newtonian contributions which can be schematically written as

$$\varphi(t) = \varphi_0(t) + \varphi_1(t) + \varphi_{1.5}(t) + \cdots . \tag{2.2}$$

Here $\varphi_0(t)$ is the dominant Newtonian part of the phase and φ_n represents the nth order post-Newtonian correction to it. In the quadrupole approximation we include only the Newtonian part of the phase given by [10]

$$\varphi(t) = \varphi_0(t) = \frac{16\pi f_a \tau_0}{5}\left[1 - \left(\frac{f}{f_a}\right)^{-5/3}\right] + \Phi, \tag{2.3}$$

where $f(t)$ is the instantaneous Newtonian gravitational wave frequency given implicitly by

$$t - t_a = \tau_0\left[1 - \left(\frac{f}{f_a}\right)^{-8/3}\right], \tag{2.4}$$

τ_0 is a constant having dimensions of time given by

$$\tau_0 = \frac{5}{256}\mathcal{M}^{-5/3}(\pi f_a)^{-8/3}, \tag{2.5}$$

and f_a and Φ are the instantaneous gravitational wave frequency and the phase of the signal, respectively, at $t = t_a$. The time elapsed starting from an epoch when the gravitational wave frequency is f_a until the epoch when it becomes infinite will be referred to as the *chirp time* of the signal. In the quadrupole approximation τ_0 is the chirp time. The Newtonian part of the phase is characterized by three parameters: (i) the *time of arrival* t_a when the signal first becomes *visible* in the detector, (ii) the *phase* Φ of the signal at the time of arrival, and (iii) the *chirp mass* $\mathcal{M} = (\mu^3 M^2)^{1/5}$, where μ and M are the reduced and the total mass of the binary, respectively. At this level of approximation two coalescing binary signals of the same chirp mass but of different sets of individual masses would be degenerate and thus exhibit exactly the same time evolution. This degeneracy is removed when post-Newtonian corrections are included.

When post-Newtonian corrections are included the parameter space of waveforms acquires an extra dimension. In this paper we show that even when post-Newtonian corrections up to relative order c^{-4}, where c is the velocity of light, are included in the phase of the waveform it is possible to make a judicious choice of the parameters so that the parameter space essentially remains only three dimensional as far as the detection problem is concerned. It should, however, be noted that the evolution of the waveform must be known to a reasonably high degree of accuracy and that further off-line analysis would be necessary to extract useful astrophysical information.

With the inclusion of corrections up to second post-Newtonian order the phase of the waveform becomes [32]

$$\varphi(t) = \varphi_0(t) + \varphi_1(t) + \varphi_{1.5}(t) + \varphi_2(t), \tag{2.6}$$

where $\varphi_0(t)$ is given by (2.3) and the various post-Newtonian contributions are given by

$$\varphi_1(t) = 4\pi f_a \tau_1\left[1 - \left(\frac{f}{f_a}\right)^{-1}\right], \tag{2.7}$$

$$\varphi_{1.5}(t) = -5\pi f_a \tau_{1.5}\left[1 - \left(\frac{f}{f_a}\right)^{-2/3}\right], \tag{2.8}$$

and

$$\varphi_2(t) = 8\pi f_a \tau_2\left[1 - \left(\frac{f}{f_a}\right)^{-1/3}\right]. \tag{2.9}$$

Now $f(t)$ is the instantaneous gravitational wave frequency correct up to second post-Newtonian order given implicitly by

$$t - t_a = \tau_0\left[1 - \left(\frac{f}{f_a}\right)^{-8/3}\right] + \tau_1\left[1 - \left(\frac{f}{f_a}\right)^{-2}\right] - \tau_{1.5}\left[1 - \left(\frac{f}{f_a}\right)^{-5/3}\right] + \tau_2\left[1 - \left(\frac{f}{f_a}\right)^{-4/3}\right]. \tag{2.10}$$

In the above equations τ's are constants having dimensions of time which depend only on the two masses of the stars and the lower frequency cutoff of the detector f_a. The total chirp time now consists of four pieces: The Newtonian contribution τ_0 is given by (2.5) and the various post-Newtonian contributions are

$$\tau_1 = \frac{5}{192\mu(\pi f_a)^2}\left(\frac{743}{336}+\frac{11}{4}\eta\right), \tag{2.11}$$

$$\tau_{1.5} = \frac{1}{8\mu}\left(\frac{m}{\pi^2 f_a^5}\right)^{1/3}, \tag{2.12}$$

and

$$\tau_2 = \frac{5}{128\mu}\left(\frac{m}{\pi^2 f_a^2}\right)^{2/3}\left(\frac{3\,058\,673}{1\,016\,064}+\frac{5429}{1008}\eta+\frac{617}{144}\eta^2\right), \tag{2.13}$$

where $\eta = \mu/M$. The phase (2.6) contains the reduced mass μ in addition to the chirp mass $\mathcal{M}$. Taking ($\mathcal{M}$, η) to be the post-Newtonian mass parameters the total mass and the reduced mass are given by $M = \mathcal{M}\eta^{-3/5}$, $\mu = \mathcal{M}\eta^{2/5}$. Note that in the total chirp time τ of the signal the 1.5 post-Newtonian contribution appears with a negative sign thus shortening the epoch of coalescence.

With the inclusion of higher order post-Newtonian corrections a chirp template is characterized by a set of four parameters which we shall collectively denote by λ^μ, $\mu = 1,\ldots,4$. At the first post-Newtonian approximation instead of working with the parameters $\lambda^\mu = \{t_a,\ \Phi,\ \mathcal{M},\ \eta\}$ we can equivalently employ the set $\{t_a,\ \Phi,\ \tau_0,\ \tau_1\}$ for the purpose of constructing templates. This, as we shall see later, has some advantages. However, at post-Newtonian orders beyond the first we do not have a unique set of chirp times to work with.

The parameters t_a and Φ are *kinematical*, which fix the origin of the measurement of time and phase, respectively, while the Newtonian and the post-Newtonian chirp times are *dynamical* parameters in the sense that they dictate the evolution of the phase and the amplitude of the signal. It may be mentioned at this stage that in most of the literature on this subject authors use the set of parameters $\{t_C,\ \Phi_C,\ \mathcal{M},\ \eta\}$ where t_C is the instant of coalescence and Φ_C is the phase of the signal at the instant of coalescence. In terms of the chirp times we have introduced, t_C is the sum of the total chirp time and the time of arrival and Φ_C is a combination of the various chirp times and Φ:

$$t_C = t_a + \tau_0 + \tau_1 - \tau_{1.5} + \tau_2, \tag{2.14}$$

$$\Phi_C = \Phi + \frac{16\pi f_a}{5}\tau_0 + 4\pi f_a\tau_1 - 5\pi f_a\tau_{1.5} + 8\pi f_a\tau_2. \tag{2.15}$$

In the stationary phase approximation the Fourier transform of the restricted second-post-Newtonian chirp waveform for positive frequencies is given by [10,13,23,20]

$$\tilde{h}(f) = \mathcal{N} f^{-7/6}\exp\left[i\sum_{\mu=1}^{6}\psi_\mu(f)\lambda^\mu - i\frac{\pi}{4}\right], \tag{2.16}$$

where

$$\mathcal{N} = A\pi^{2/3}\left(\frac{2\tau_0}{3}\right)^{1/2} f_a^{4/3}$$

is a normalization constant, λ^μ, $\mu = 1,\ldots,6$, represent the various post-Newtonian parameters

$$\lambda^\mu = \{t_a, \Phi, \tau_0, \tau_1, \tau_{1.5}, \tau_2\} \tag{2.17}$$

and

$$\psi_1 = 2\pi f, \tag{2.18}$$

$$\psi_2 = -1, \tag{2.19}$$

$$\psi_3 = 2\pi f - \frac{16\pi f_a}{5} + \frac{6\pi f_a}{5}\left(\frac{f}{f_a}\right)^{-5/3}, \tag{2.20}$$

$$\psi_4 = 2\pi f - 4\pi f_a + 2\pi f_a\left(\frac{f}{f_a}\right)^{-1}, \tag{2.21}$$

$$\psi_5 = -2\pi f + 5\pi f_a - 3\pi f_a\left(\frac{f}{f_a}\right)^{-2/3}, \tag{2.22}$$

$$\psi_6 = 2\pi f - 8\pi f_a + 6\pi f_a\left(\frac{f}{f_a}\right)^{-1/3}. \tag{2.23}$$

For $f < 0$ the Fourier transform is computed using the identity $\tilde{h}(-f) = \tilde{h}^*(f)$ obeyed by real functions $h(t)$. In addition to the above-mentioned parameters we shall introduce an amplitude parameter $\mathcal{A}$ in Sec. III.

III. A GEOMETRIC APPROACH TO SIGNAL ANALYSIS

In this section we apply the techniques of differential geometry to the problem of detecting weak signals embedded in noise. In Sec. III A we elaborate on the concept of the signal manifold and comment on the relationship of this approach with that of Amari [19]. Our discussion of the vector space of all detector outputs is modeled after the discussion given in [33]. (Also see [20] for the geometrical concepts in signal analysis and [21] for application to search algorithms.) In Sec. III B we deal with the problem of choosing a set of filters for online analysis which would optimize the task of detection of the signal. In Sec. III C we deal with the dimensionality of the chirp manifold when we incorporate higher order post-Newtonian corrections. It is found that due to covariances between the parameters, it is possible to introduce an effective dimension which is less than the dimension of the manifold. This has very important implications for the detection problem.

A. Signal manifold

The output of a gravitational wave detector such as the LIGO will comprise of data segments, each of duration T seconds, uniformly sampled with a sampling interval of Δ, giving the number of samples in a single data train to be $N = T/\Delta$. Each data train can be considered as an N-tuple $(x^0, x^1, \ldots, x^{N-1})$, x^k being the value of the output of the detector at time $k\Delta$. The set of all such N-tuples constitutes an N-dimensional vector space $\mathcal{V}$ where the addition of two vectors is accomplished by the addition of corresponding time samples. For later convenience we allow each sample to take complex values.

A natural basis for this vector space is the *time basis* $\mathbf{e}^k_m = \delta^k_m$ where m and k are the vector and component indices, respectively. Another basis which we shall use extensively is the Fourier basis which is related to the time basis by a unitary transformation $\hat{U}$:

$$\tilde{\mathbf{e}}_m = \hat{U}^{mn}\mathbf{e}_n = \frac{1}{\sqrt{N}}\sum_{n=0}^{N-1}\mathbf{e}_n \exp\left[\frac{2\pi imn}{N}\right], \tag{3.1}$$

$$\mathbf{e}_m = \hat{U}^{\dagger mn}\tilde{\mathbf{e}}_n = \frac{1}{\sqrt{N}}\sum_{n=0}^{N-1}\tilde{\mathbf{e}}_n \exp\left[-\frac{2\pi imn}{N}\right]. \tag{3.2}$$

All vectors in $\mathcal{V}$ are shown in boldface, and the Fourier basis vectors and components of vectors in the Fourier basis are highlighted with a "tilde."

In the continuum case each data train can be expanded in a Fourier series and will contain a finite number of terms in the expansion, as the output will be band limited. The expansion is carried out over the exponential functions $\exp(2\pi imt/T)$ which are precisely the Fourier basis vectors defined above. Though the index m takes both positive and negative values corresponding to positive and negative frequencies, it is both possible and convenient to allow m to take only positive values [34]. Thus the vector space $\mathcal{V}$ can be considered as being spanned by the N Fourier basis vectors, implying immediately that the number of independent vectors in the time basis to be also N. This is the content of the Nyquist theorem which states that it is sufficient to sample the data at a frequency which is twice as large as the bandwidth of a real-valued signal, where the bandwidth refers to the range of positive frequencies over which the signal spectrum is nonzero. This factor of 2 does not appear in the vector space picture as we allow in general for complex values for the components in the time basis.

A gravitational wave signal from a coalescing binary system can be characterized by a set of parameters $\boldsymbol{\lambda} = (\lambda^0, \lambda^1, \ldots, \lambda^{p-1})$ belonging to some open set of the p-dimensional real space R^p. The set of such signals, $\mathbf{s}(t;\boldsymbol{\lambda})$, constitutes a p-dimensional manifold $\mathcal{S}$ which is embedded in the vector space $\mathcal{V}$. The parameters of the binary act as coordinates on the manifold. The basic problem of signal analysis is thus to determine whether the detector output vector $\mathbf{x}$ is the sum of a signal vector and a noise vector, $\mathbf{x} = \mathbf{s} + \mathbf{n}$, or just the noise vector, $\mathbf{x} = \mathbf{n}$, and furthermore to identify which particular signal vector, among all possible. One would also like to estimate the errors in such a measurement.

In the absence of the signal the output will contain only noise drawn from a stochastic process which can be described by a probability distribution on the vector space $\mathcal{V}$. The covariance matrix of the noise C^{jk} is defined as

$$C^{jk} = \overline{n^j n^{*k}}, \tag{3.3}$$

where an asterisk denotes complex conjugation and an overbar denotes an average over an ensemble. If the noise is assumed to be stationary and ergodic, then there exists a noise correlation function $K(t)$ such that $C_{jk} = K(|j-k|\Delta)$. In the Fourier basis it can be shown that the components of the noise vector are statistically independent [11] and the covariance matrix in the Fourier basis will contain only diagonal terms whose values will be strictly positive: $\tilde{C}_{jj} = \tilde{n}^j\tilde{n}^{*j}$. This implies that the covariance matrix has strictly positive eigenvalues. The diagonal elements of this matrix $\tilde{C}_{jj}$ constitute the discrete representation of the power spectrum of the noise $S_n(f)$.

We now discuss how the concept of matched filtering can be used to induce a metric on the signal manifold. The technique of matched filtering involves correlating the detector output with a bank of filters, each of which is tuned to detect the gravitational wave from a binary system with a particular set of parameters. The output of the filter, with an impulse response $\mathbf{q}$, is given in the discrete case as

$$c_{(m)} = \frac{1}{\sqrt{N}}\sum_{n=0}^{N-1}\tilde{x}^n\tilde{q}^{*n}\exp[-2\pi imn/N]. \tag{3.4}$$

The SNR (ρ) at the output is defined to be the mean of $c_{(m)}$ divided by the square root of its variance:

$$\rho \equiv \frac{\overline{c_{(m)}}}{\left[\overline{\left(c_{(m)} - \overline{c_{(m)}}\right)^2}\right]^{1/2}}. \tag{3.5}$$

By maximizing ρ we can obtain the expression for the optimal filter $\mathbf{q}_{(m)}$ matched to a particular signal $\mathbf{s}(t;\lambda^\mu)$ as

$$\tilde{q}^n_{(m)}(\lambda^\mu) = \frac{\tilde{s}^n(\lambda^\mu)\exp[2\pi imn/N]}{\tilde{C}_{nn}}, \tag{3.6}$$

where ρ has been maximized at the mth data point at the output and where $\mu = 1, 2, \ldots, p$, where p is the number of parameters of the signal. We now introduce a scalar product in $\mathcal{V}$. For any two vectors $\mathbf{x}$ and $\mathbf{y}$,

$$\langle \mathbf{x}, \mathbf{y}\rangle = \sum_{i,j=0}^{N-1} C^{-1}_{ij}x^i y^j = \sum_{n=0}^{N-1}\frac{\tilde{x}^n\tilde{y}^{*n}(\lambda^\mu)}{\tilde{C}_{nn}}. \tag{3.7}$$

In terms of this scalar product, the output of the optimal filter $\mathbf{q}$, matched to a signal $\mathbf{s}(\lambda^\mu)$, can be written as

$$c_{(m)}(\lambda^\mu) = \frac{1}{\sqrt{N}}\langle \mathbf{x}, \mathbf{s}\rangle. \tag{3.8}$$

As $\tilde{C}_{kk}$ is strictly positive the scalar product defined is positive definite. The scalar product defined above on the vector space $\mathcal{V}$ can be used to define a norm on $\mathcal{V}$ which in turn can be used to induce a metric on the manifold. The norm of a vector $\mathbf{x}$ is defined as $\|\mathbf{x}\| = \langle \mathbf{x}, \mathbf{x}\rangle^{1/2}$. The norm for the optimal filter can be calculated to give $\rho = \langle \mathbf{s}, \mathbf{s}\rangle^{1/2}$. The norm of the noise vector will be a random variable $\langle \mathbf{n}, \mathbf{n}\rangle^{1/2}$ with a mean value of $\sqrt{N}$ as can be seen by writing the expression for the norm of the noise vector and subsequently taking an ensemble average.

The distance between two points infinitesimally separated on $\mathcal{S}$ can be expressed as a quadratic form in the differences in the values of the parameters at the two

points:

$$g_{\mu\nu}d\lambda^\mu d\lambda^\nu \equiv \|\mathbf{s}(\lambda^\mu + d\lambda^\mu) - \mathbf{s}(\lambda^\mu)\|^2 = \left\| \frac{\partial \mathbf{s}}{\partial \lambda^\mu} d\lambda^\mu \right\|^2 \tag{3.9}$$

$$= \left\langle \frac{\partial \mathbf{s}}{\partial \lambda^\mu}, \frac{\partial \mathbf{s}}{\partial \lambda^\nu} \right\rangle d\lambda^\mu d\lambda^\nu. \tag{3.10}$$

The components of the metric in the coordinate basis are seen to be the scalar products of the coordinate basis vectors of the manifold.

Since the number of correlations we can perform online is finite, we cannot have a filter corresponding to every signal. A single filter though matched to a particular signal will also "detect" signals in a small neighborhood of that signal but with a slight loss in the SNR. The metric on the manifold quantifies the drop in the correlation in a neighborhood of the signal chosen. Taking the output vector to be $\mathbf{x}$ and two signal vectors $\mathbf{s}(\boldsymbol{\lambda})$ and $\mathbf{s}(\boldsymbol{\lambda} + \mathbf{d}\boldsymbol{\lambda})$ and using Schwarz's inequality we have

$$\langle \mathbf{x}, \mathbf{s}(\boldsymbol{\lambda} + d\boldsymbol{\lambda}) \rangle - \langle \mathbf{x}, \mathbf{s}(\boldsymbol{\lambda}) \rangle = \langle \mathbf{x}, \mathbf{s}(\boldsymbol{\lambda} + d\boldsymbol{\lambda}) - \mathbf{s}(\boldsymbol{\lambda}) \rangle \leq \|\mathbf{x}\| \|\mathbf{s}(\boldsymbol{\lambda} + d\boldsymbol{\lambda}) - \mathbf{s}(\boldsymbol{\lambda})\| \tag{3.11}$$

$$= \|\mathbf{x}\| g_{\mu\nu} d\lambda^\mu d\lambda^\nu. \tag{3.12}$$

As is apparent the drop in the correlation can be related to the metric distance on the manifold between the two infinitesimally separated signal vectors.

We now discuss Amari's [19] work in the context of using differential geometry in statistics and elaborate on the relationship with the approach we have taken. The set of parametrized probability distributions corresponding to a statistical model constitute a manifold. The parametrized probability distributions in the context of a signal analysis of gravitational waves from coalescing binaries are the ones which specify the probability that the output vector will lie in a certain region of the vector space $\mathcal{V}$ given that a signal $\mathbf{s}(t; \boldsymbol{\lambda})$ exists in the output which we denote as $p(\mathbf{x}|\mathbf{s}(t; \boldsymbol{\lambda}))$ Since it is not our intention to develop Amari's approach any further, we will be brief and will make all the mathematical assumptions such as infinite differentiability of functions, interchangeability of the differentiation, expectation value operators, etc.

The set of probability distributions $p(\mathbf{x}|\mathbf{s}(\boldsymbol{\lambda}))$, where $\boldsymbol{\lambda} \in R^p$, constitutes a manifold $\mathcal{P}$ of dimension p. At every point on this manifold we can construct a tangent space T^0 on which we can define the coordinate basis vectors as $\partial_\mu = \frac{\partial}{\partial \lambda^\mu}$. Any vector $\mathbf{A}$ in this tangent space can be written as a linear combination of these coordinate basis vectors. We now define p random variables $\sigma_\mu = -\frac{\partial}{\partial \lambda^\mu} \ln[p(\mathbf{x}|\mathbf{s}(\boldsymbol{\lambda}))]$. It can easily be shown that $\overline{\sigma_\mu} = 0$. We assume that these p random variables are linearly independent. By taking all possible linear combinations of these random variables we can construct another linear space T^1. Each vector $\mathbf{B}$ in T^1 can be written as $\mathbf{B} = B^\mu \sigma_\mu$. The two vector spaces T^0 and T^1 are isomorphic to each other, which can be shown explicitly by making the correspondence $\sigma_\mu \leftrightarrow \partial_\mu$. The vector space T^1 has a natural inner product defined on it which is the covariance matrix of the p random variables σ_μ. This scalar product can be carried over to T^0 using the correspondence stated above. The metric on the manifold can be defined by taking the scalar product of the coordinate basis vectors

$$g_{\mu\nu} = \langle \partial_\mu, \partial_\nu \rangle = \overline{\sigma_\mu \sigma_\nu}. \tag{3.13}$$

In statistical theory the above matrix $g_{\mu\nu}$ is called the Fisher information matrix. We will also denote the Fisher matrix, as is conventional, by $\Gamma_{\mu\nu}$. It is clearly seen that orthogonality between vectors in the tangent space of the manifold is related to statistical independence of random variables in T^1.

If we take the case of Gaussian noise, the metric defined above is identical to the one obtained on the signal manifold by matched filtering. Gaussian noise can be described by the distribution

$$p(\mathbf{n}) = \frac{\exp\left[-\frac{1}{2}\sum_{j,k=0}^{N-1} C^{-1}_{jk} n^j n^{k*}\right]}{\{(2\pi)^N \det[C_{jk}]\}^{1/2}} = \frac{\exp\left[-\frac{1}{2}\sum_{j,k=0}^{N-1} \tilde{C}^{-1}_{jk} \tilde{n}^j \tilde{n}^{k*}\right]}{\left\{(2\pi)^N \det\left[\tilde{C}_{jk}\right]\right\}^{1/2}} = \frac{\exp\left[-\frac{1}{2}\sum_{j=0}^{N-1} \frac{\tilde{n}^j \tilde{n}^{j*}}{\tilde{C}_{jj}}\right]}{\left\{(2\pi)^N \det\left[\tilde{C}_{jk}\right]\right\}^{1/2}}, \tag{3.14}$$

where in the last step we have used the diagonal property of the matrix $\tilde{C}^{jk}$ which implies that $\tilde{C}^{-1}_{jj} = 1/\tilde{C}_{jj}$.

As the noise is additive $p(\mathbf{x}|\mathbf{s}(\boldsymbol{\lambda}))$ can be written as $p(\mathbf{x} - \mathbf{s}(\boldsymbol{\lambda}))$. Assuming Gaussian noise we can write the expressions for the random variables σ_μ as

$$\sigma_\mu = \left(\frac{1}{2}\right) \frac{\partial}{\partial \lambda^\mu} \langle \mathbf{x} - \mathbf{s}(\boldsymbol{\lambda}), \mathbf{x} - \mathbf{s}(\boldsymbol{\lambda}) \rangle = \left\langle \mathbf{n}, \frac{\partial}{\partial \lambda^\mu} \mathbf{s}(\boldsymbol{\lambda}) \right\rangle, \tag{3.15}$$

where in the last step we have used $\mathbf{x} = \mathbf{s}(\boldsymbol{\lambda}) + \mathbf{n}$. The covariance matrix for the random variables σ_μ can be calculated to give

$$\overline{\sigma_\mu \sigma_\nu} = \left\langle \frac{\partial}{\partial \lambda^\mu} \mathbf{s}(\boldsymbol{\lambda}), \frac{\partial}{\partial \lambda^\nu} \mathbf{s}(\boldsymbol{\lambda}) \right\rangle, \tag{3.16}$$

which is the same metric as defined over the signal manifold. Thus, both the manifolds $\mathcal{S}$ and $\mathcal{P}$ are identical with

respect to their metrical properties. We will henceforth restrict our attention to the signal manifold $\mathcal{S}$.

For the purpose of our analysis we will choose a minimal set of parameters characterizing the gravitational wave signal from a coalescing binary. We consider only the first post-Newtonian corrections. In Sec. II we have already introduced the four parameters $\lambda^\mu = \{t_a, \Phi, \tau_0, \tau_1\}$. We now introduce an additional parameter for the amplitude and call it $\lambda^0 = \mathcal{A}$. The signal can now be written as $\tilde{s}(f;\boldsymbol{\lambda}) = \mathcal{A}h(f; t_a, \Phi, \tau_0, \tau_1)$, where $\boldsymbol{\lambda} \equiv \{\mathcal{A}, t_a, \Phi, \tau_0, \tau_1\}$. Numerically the value of the parameter $\mathcal{A}$ will be the same as that of the SNR obtained for the matched filter provided $\mathbf{h}$ has unit norm. We can decompose the signal manifold into a manifold containing normalized chirp waveforms and a one-dimensional manifold corresponding to the parameter $\mathcal{A}$. The normalized chirp manifold can therefore be parametrized by $\{t_a, \Phi, \tau_0, \tau_1\}$. This parametrization is useful as the coordinate basis vector $\frac{\partial}{\partial \mathcal{A}}$ will be orthogonal to all the other basis vectors as will be seen below.

In order to compute the metric and equivalently the Fisher information matrix, we use the continuum version of the scalar product as given in [22], except that we use the two-sided power spectral density. This has the advantage of showing clearly the range of integration in the frequency space though we get the same result using the discrete version of the scalar product. Using the definition of the scalar product we get

$$g_{\mu\nu} = \int_{f_a}^{\infty} \frac{df}{S_n(f)} \frac{\partial \tilde{s}(f;\boldsymbol{\lambda})}{\partial \lambda^\mu} \frac{\partial \tilde{s}^*(f;\boldsymbol{\lambda})}{\partial \lambda^\nu} + \text{c.c.} \tag{3.17}$$

Recall that in the stationary phase approximation the Fourier transform of the coalescing binary waveform is given by $\tilde{h}(f,\boldsymbol{\lambda}) = \mathcal{N} f^{-7/6} \exp\left[i \sum_\mu \psi_\mu(f) \lambda^\mu\right]$ and $\tilde{s}(f) = \mathcal{A}\tilde{h}(f)$, where $\psi_\mu(f)$ are given by Eqs. (2.18)–(2.23), $\mu = 1, \ldots, 4$, and $\lambda^\mu = \{t_a,\ \Phi,\ \tau_0,\ \tau_1\}$. Note, in particular, that in the phase of the waveform the parameters occur linearly, thus enabling a very concise expression for the components of $g_{\mu\nu}$. The various partial derivatives are given by

$$\frac{\partial \tilde{s}(f;\boldsymbol{\lambda})}{\partial \lambda^\mu} = i\psi_\mu(f)\tilde{s}(f;\boldsymbol{\lambda}), \tag{3.18}$$

where we have introduced $\psi_0 = -i/\mathcal{A}$. On substituting the above expressions for the partial derivatives in Eq. (3.17) we get

$$g_{\mu\nu} = \langle \psi_\mu h, \psi_\nu h \rangle = 2 \int_{f_a}^{\infty} \frac{\psi_\mu(f)\psi_\nu^*(f) \left|\tilde{h}(f,\boldsymbol{\lambda})\right|^2}{S_n(f)} df. \tag{3.19}$$

The above definition of the amplitude parameter $\mathcal{A}$, as in Culter and Flannagan [20], disjoins the amplitude of the waveform from the rest of the parameters. Since ψ_0 is pure imaginary and ψ_μ's are real, it is straightforward to see from Eq. (3.19) that

$$g_{00} = 1 \text{ and } g_{0\mu} = 0, \quad \mu = 1, \ldots, 4. \tag{3.20}$$

The rest of the components $g_{\mu\nu}$ are seen to be independent of all the parameters except $\mathcal{A}$, i.e., $g_{\mu\nu} \propto \mathcal{A}^2$. As $\mathcal{A}$ is unity for the normalized manifold the metric on the normalized manifold is flat. This implies not only that the manifold is intrinsically flat (in the stationary phase approximation) but also that the coordinate system used is Cartesian. If instead of the chirp times (τ_0, τ_1) we use the parameter $(\mathcal{M}, \mu)$, then the metric coefficients will involve these parameters and the coordinate system will no longer remain Cartesian.

B. Choice of filters

We now use the differential geometric formalism to tackle the issue of optimal filter placement. Until now, it has been thought necessary to use a finite subset of the set of chirp signals as templates for detection. We show that this is unduly restrictive. We suggest a procedure by which the detection process can be made more "efficient" by moving the filters out of the manifold. It must be emphasized that the algorithm presented below is both simplistic and quite *ad hoc* and is not necessarily the best. Moreover, we have implemented the algorithm only for the Newtonian case where the computational requirements are not very heavy. However, the signal manifold corresponding to post-Newtonian waveform will be a larger dimensional manifold and there the computational requirements will be substantial. The choice of optimal filters which span the manifold will then be crucial.

Detection of the coalescing binary signal involves computing the scalar product of the output of the detector with the signal vectors. Subsequently one would have to maximize the correlations over the parameters and the number so obtained would serve as the statistic on the basis of which we can decide whether a signal is present in the given data train. Geometrically, this maximization corresponds to minimizing the angle between the output vector and the vectors corresponding to the normalized signal manifold. Using the cosine formula

$$\cos(\theta) = \frac{\langle \mathbf{s}(\boldsymbol{\lambda}), \mathbf{x} \rangle}{\|\mathbf{x}\| \|\mathbf{s}(\boldsymbol{\lambda})\|} = \frac{\|\mathbf{s}(\boldsymbol{\lambda})\|^2 + \|\mathbf{x}\|^2 - \|\mathbf{x} - \mathbf{s}(\boldsymbol{\lambda})\|^2}{2\|\mathbf{x}\| \|\mathbf{s}(\boldsymbol{\lambda})\|} \tag{3.21}$$

and the fact that $\|\mathbf{s}(\boldsymbol{\lambda})\|$ is unity for the vectors belonging to the normalized signal manifold, maximizing the scalar product is equivalent to minimizing $\|\mathbf{x} - \mathbf{s}(\boldsymbol{\lambda})\|$ which is the distance between the tip of the output vector and the manifold.

Given the constraints of computational power one would be able to evaluate only a finite number of these scalar products, say, n_F, in a certain amount of time depending on the length of the data train. It is therefore necessary to be able to choose the n_F filters in such a manner that the detection probability is maximal. We will need efficient on-line data analysis for two reasons: (i) to isolate those data trains which have a high probability of containing a signal and (ii) to determine the parameters of the binary early on during the inspiral and to use them for dynamical recycling techniques [35]. Be-

cause of the finiteness of the filter spacing, the signal parameters will in general not correspond to any of the n_F filters chosen and this will lead to a drop in the maximum possible correlation. Until now attention has been focused on identifying an optimal set of filters which are a discrete subset of the manifold. If detection is the sole purpose, then the differential geometric picture suggests that confining the filter vectors to the signal manifold is an unnecessary restriction and in fact nonoptimal. Thus it is worthwhile to explore making a choice of filters outside the manifold. The filter vectors will thus belong to $\mathcal{V}$ but will not, in general, correspond to any signal. It is, of course, true that we are sacrificing on the maximum possible correlation obtainable (when the signal's parameters coincide with those of the filter). Thus the problem essentially is to select n_F filter vectors which optimize the detection the efficiency of which depends upon the properties of the manifold.

In general a single filter vector would have to pick up signals over a region of the manifold. The extent of this region is determined by fixing a threshold on the correlation between the filter and any signal in the region. We will denote this threshold by κ, where κ takes a value which is close to, but less than, unity. The typical value suggested for κ is ~ 0.8 [13]. For a given filter $\mathbf{q}$ and a threshold κ the region on the manifold corresponding to the filter will be denoted as $\mathcal{S}_{\mathbf{q}}(\kappa)$, where $\mathcal{S}_{\mathbf{q}}(\kappa) \subset \mathcal{S}$. Geometrically this region is the intersection of the manifold and an open ball of radius $2^{1/2}(1-\kappa)^{1/2}$ with center $\mathbf{q}$ in $\mathcal{V}$. The n_F filters taken together would have to "span" the manifold which means that the union of the regions covered by each filter would be the manifold itself, i.e., $\bigcup_{\mathbf{q}} \mathcal{S}_{\mathbf{q}}(\kappa) = \mathcal{S}$. If the filter $\mathbf{q}$ lies on the manifold, then the correlation function $c_{\mathbf{q}}(\boldsymbol{\lambda}) = \langle \mathbf{s}(\boldsymbol{\lambda}), \mathbf{q} \rangle$ will reach its maximum value of unity in $\mathcal{S}_{\mathbf{q}}(\kappa)$ when $\mathbf{q} = \mathbf{s}(\boldsymbol{\lambda})$ and will fall off in all directions. This means that the signals in the region which are farther away from the filter are less likely to be picked up as compared to those in the immediate neighborhood of the filter $\mathbf{q}$.

We assume that a finite subset of the normalized signal manifold has been chosen to act as filters by some suitable algorithm [13], which taken together span the manifold. The number of filters will be determined by the available computing power. Consider one of these filters $\mathbf{q}$, the region corresponding to it for a threshold of κ, $\mathcal{S}_{\mathbf{q}}(\kappa)$, and an arbitrary normalized vector $\mathbf{q}_0$ which belongs to $\mathcal{V}$ but not necessarily $\mathcal{S}$. By correlating the vector $\mathbf{q}_0$ with vectors in $\mathcal{S}_{\mathbf{q}}(\kappa)$ we obtain the correlation function $c_{\mathbf{q}_0}(\boldsymbol{\lambda}) = \langle \mathbf{s}(\boldsymbol{\lambda}), \mathbf{q}_0 \rangle$. The optimal filter $\mathbf{q}_0$ is chosen such that it maximizes the average of the correlation function:

$$\langle \mathbf{s}(\boldsymbol{\lambda}), \mathbf{q}_0 \rangle_{\mathrm{av}} = \frac{1}{\int_{\mathcal{S}_{\mathbf{q}}(\eta)} \sqrt{g} d^p\lambda} \int_{\mathcal{S}_{\mathbf{q}}(\eta)} \langle \mathbf{s}(\boldsymbol{\lambda}), \mathbf{q}_0 \rangle \sqrt{g} d^p\lambda = \left\langle \int_{\mathcal{S}_{\mathbf{q}}(\eta)} \mathbf{s}(\boldsymbol{\lambda}) d^p\lambda \ , \ \mathbf{q}_0 \right\rangle , \tag{3.22}$$

where $g = \det[g_{\mu\nu}]$. In the last step above the integration and the scalar product operations have been interchanged. Moreover, for the normalized chirp manifold the metric does not depend upon the parameters in the coordinate system we have chosen, and therefore $g_{\mu\nu}$ is a constant and the factor $\sqrt{g}$ cancels. We now use Schwarz's inequality to maximize the average correlation to obtain

$$\mathbf{q}_0 = \mathcal{N} \int_{\mathcal{S}_{\mathbf{q}}(\kappa)} \mathbf{s}(\boldsymbol{\lambda}) d^p\lambda, \tag{3.23}$$

where $\mathcal{N}$ is a normalization constant.

We implemented the above algorithm for filter placement for the case of Newtonian signals with certain modifications. The normalized chirp waveform consists of three parameters (Φ, t_a, τ_0). If we keep t_a and τ_0 fixed, then the tip of the signal vector traces out a circle as we vary Φ. As any circle lies on a plane we can express a signal vector as a linear sum of two vectors where the two vectors differ only in the phase parameter and we take this phase difference to be $\pi/2$. Thus, we need only two mutually orthogonal filters to span the phase parameter. The time of arrival parameter t_a is also a "convenient parameter" as by the use of fast Fourier transforms the correlations for arbitrary time of arrival can be performed at one go. It is therefore not profitable for us to maximize the average correlation over the phase parameter Φ and the time of arrival t_a.

In view of the above restrictions we modified the filter placement algorithm. We consider the correlation function for the case when the filter vector is on the manifold. We define the "line of curvature" to be the curve on the manifold along which the correlation function falls the least. Figure 1 illustrates the correlation function plotted as a function of τ_0 along the line of curvature. It is seen from the contour diagram of the numerically computed correlation function that the line of curvature lies nearly on the submanifold $t_a + \tau_0 = \text{const}$, of the normalized chirp manifold. We take two curves passing through the point $\mathbf{q}$ in the region $\mathcal{S}_{\mathbf{q}}(\eta)$: (1) $t_a + \tau_0 = \text{const}$, $\Phi = 0$, and (2) $t_a + \tau_0 = \text{const}$, $\Phi = \pi/2$. We obtain one filter for each of the two curves by evaluating Eq. (3.23) where the domains of integration correspond to the segments of the curves defined.

Having determined the two filters we again plot the correlation function along the line of curvature as a function of τ_0 in Fig. 1. The region of the manifold selected corresponds to a range of 5.8–6.0 s in the parameter τ_0. Similar curves will be obtained if we shift the range of values taken in τ_0 by a constant amount as the correlation function depends only on the difference in the values of τ_0. It can be seen that the correlation has a minimum at the center. In order to get a flatter correlation curve we select a linear combination of the original filter and the one obtained by averaging, with suitable weights at-

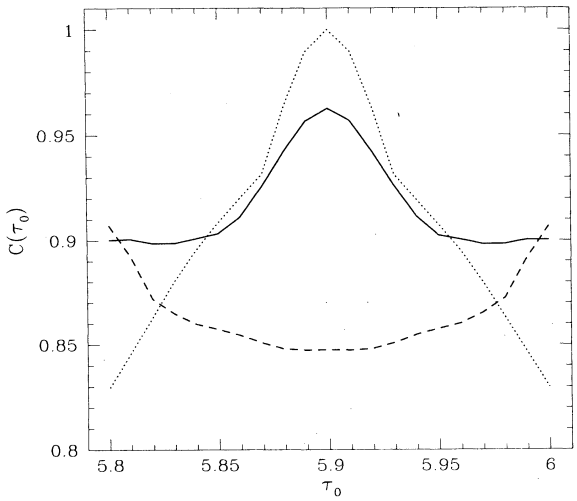

FIG. 1. This figure illustrates the correlation function along the line of curvature as a function of τ_0, the Newtonian chirp time, for the following three cases: (i) when the filter is placed on the manifold (dotted line), (ii) when the filter is the "average" signal vector over the region (dashed line), and (iii) when the filter is chosen to be an appropriate linear combination of the previous two filters (solid line).

tached to each filter. This performs reasonably well as shown by the thick curve in the figure. The importance of having a flatter correlation function lies in the fact that all the signals in a region can be picked up with equal efficiency and the drop in the maximum possible correlation can be compensated for by lowering the threshold. The average correlation obtained for the optimal filter is only marginally better than that obtained for the filter placed on the manifold.

In the discussion above, we had started with a fixed number of filters, n_F, on the manifold and obtained another set of n_F filters which performs marginally better than the former set. Equivalently, we can try to increase the span of each filter, retaining the same threshold but reducing the number of filters required. In Fig. 1 we observe that the optimal filter chosen spans the entire region considered with a threshold greater than 0.9, whereas the filter on the manifold spans about half the region at the same threshold. This indicates that by moving the filters out of the manifold it may be possible to reduce the number of filters by a factor of 2 or so. One must, however, bear in mind that the bank of filters obtained in this way is not optimal. There is scope to improve the scheme further and our analysis is indicative of this feature.

C. Effective dimensionality of the parameter space of a second order post-Newtonian waveform

It has already been shown that the first post-Newtonian waveform is essentially one dimensional [29]. We argue in this subsection that even the second post-Newtonian waveform is essentially one dimensional and a one-dimensional lattice suffices to filter the waveform.

A Newtonian waveform is characterized by a set of three parameters consisting of the time of arrival, the phase of the signal at the time of arrival, and the chirp mass (or, equivalently, the Newtonian chirp time). In this case, for the purpose of detection, one essentially needs to employ a one-dimensional lattice of filters corresponding to the chirp mass, the time of arrival being taken care by the fast Fourier transform algorithm and the phase being determined using a two-dimensional basis of orthogonal templates. When post-Newtonian corrections are included in the phase of the waveform the number of parameters increases, apparently implying that one needs to use a two-dimensional lattice of filters corresponding to, say, the chirp and reduced masses (equivalently the Newtonian and post-Newtonian chirp times) which in turn means that the number of templates through which the detector output needs to be filtered goes up by several orders of magnitude. One of us (B.S.S.) has recently shown that for the purpose of detection it is sufficient to use a one-dimensional lattice of filters even after first post-Newtonian corrections are included in the phase of the waveform and the relevant parameter here is the sum of the Newtonian and post-Newtonian chirp times. What happens when corrections beyond the first post-Newtonian order are incorporated in the phase of the waveform?

The coalescing binary waveform is now available up to second post-Newtonian order [32,36]. Blanchet *et al.* argue that the phase correction due to the second order post-Newtonian (2PN) term induces an accumulated difference of 10 cycles in a total of 16 000. Consequently, it is important to incorporate the 2PN terms in the templates. When the 2PN terms are included it is useful to consider that the full waveform is parametrized by three additional parameters, corresponding to the chirp times at the 1PN, 1.5PN, and 2PN order (cf. Sec. II). Of course, as far as the detection problem is concerned there is only one additional parameter since the chirp times are all functions of the two masses of the binary. However, for the purpose of testing general relativity one can consider each of the chirp times to be independent of the rest [5,24]. Our problem now is to find the dimensionality of the parameter space of a 2PN waveform. To this end we consider the *ambiguity function* $C(\boldsymbol{\lambda}', \boldsymbol{\lambda})$ which is nothing but the correlation function of two normalized waveforms one of whose parameters $\boldsymbol{\lambda}$ are varied by holding the parameters of the other fixed $\boldsymbol{\lambda}'$:

$$C(\boldsymbol{\lambda}', \boldsymbol{\lambda}) = \langle q(\boldsymbol{\lambda}'), q(\boldsymbol{\lambda}) \rangle ,$$
$$\langle q(\boldsymbol{\lambda}'), q(\boldsymbol{\lambda}') \rangle = \langle q(\boldsymbol{\lambda}'(\boldsymbol{\lambda}) \rangle = 1. \qquad (3.24)$$

It is useful to think of $\boldsymbol{\lambda}'$ as the parameters of a template and $\boldsymbol{\lambda}$ as that of a signal. With this interpretation the ambiguity function simply gives the span of a filter in the parameter space.

The ambiguity function for the full waveform is a four-dimensional surface since there are four independent parameters. To explore the effective dimensionality of the parameter we consider the set of parameters to be $\{t_a, \Phi, m_1, m_2\}$, where m_1 and m_2 are the two masses of the binary. We have shown the contours of the ambiguity function maximized over t_a and

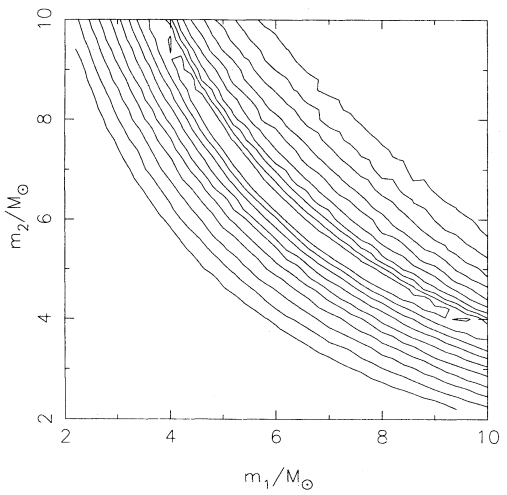

FIG. 2. Contour diagram of the ambiguity function for the second post-Newtonian case.

Φ (since these two parameters do not explicitly need a lattice of templates) in Fig. 2. The template at the center of the plot corresponds to a binary waveform with $m_1 = m_2 = 1.4M_\odot$ and the signal parameters are varied over the entire astrophysically interesting range of masses: $m_1, m_2 \in [1.4, 10]M_\odot$. From this figure we find that the ambiguity function is almost a constant along a particular line in the m_1-m_2 plane. This means that a template at the center of the grid spans a relatively large area of the parameter space by obtaining a correlation very close to unity for all signals whose masses lie on the curve along which the ambiguity function roughly remains a constant. It turns out that the equation of this curve is given by

$$\tau_0 + \tau_1 - \tau_{1.5} + \tau_2 = \text{const.} \tag{3.25}$$

Let us suppose we begin with a two-dimensional lattice of filters corresponding to a certain grid (albeit, nonuniform) laid in the m_1-m_2 plane. Several templates of this set will have their total chirp time the same. Now with the aid of just one template, out of all those that have the same chirp time, we can effectively span the region that is collectively spanned by all such filters. More precisely, we will not have an appreciable loss in the SNR in replacing all templates of a given total chirp time by one of them. Consequently, the signal manifold can be spanned by a one-dimensional lattice of templates.

IV. ESTIMATION OF PARAMETERS

In this section we discuss the accuracy at which the various parameters of a coalescing binary system of stars can be estimated. All our results are for a single interferometer of the initial LIGO type which has a lower frequency cutoff at 40 Hz. At present it is beyond the computer resources available to us to carry out a simulation for the advanced LIGO. In the first part of this section we briefly review the well-known results obtained for the variances and covariances in the estimation of parameters using analytical methods. Analytical methods assume that the SNR is sufficiently large (the so-called strong signal approximation) and implicitly use a continuum of the parameter space. In reality, however, these assumptions are not necessarily valid and hence it is essential to substantiate the results obtained using analytical means by performing numerical simulations. In the second part of this section we present an exhaustive discussion of the Monte Carlo simulations we have performed to compute the errors and covariances of different parameters. As we shall discuss below the computation of errors using the covariance matrix is erroneous even at a SNR of 10–20. Our estimation of 1σ uncertainty in the various parameters, at low SNR's, is substantially larger than those computed using the covariance matrix. However, for high values of the SNR (> 25–30) Monte Carlo estimation agrees with the analytical results.

A. Covariance matrix

In recent years a number of authors has addressed issues related to the variances expected in parameter estimation [5,18,22,23,20,24–28,37]. In the standard method of computing the variances in the estimation of parameters one makes the assumption that the SNR is so large that with the aid of such an approximation one can first construct the Fisher information matrix $\Gamma_{\mu\nu}$ and then take its inverse to obtain the covariance matrix $C_{\mu\nu}$. In the strong signal approximation the Fisher information matrix and the covariance matrix are given by

$$g_{\mu\nu} = \Gamma_{\mu\nu} = \left\langle \frac{\partial \mathbf{s}}{\partial \lambda^\mu}, \frac{\partial \mathbf{s}}{\partial \lambda^\nu} \right\rangle, \quad C_{\mu\nu} = \Gamma^{-1}\mu\nu. \tag{4.1}$$

As we have seen before the Fisher information, and consequently the covariance matrix, is block diagonal and hence there is no cross talk, implying vanishing of the covariances between the amplitude and the other parameters. Consequently, we need not construct, for the purpose of Weiner filtering, templates corresponding to different amplitudes.

For the purpose of numerical simulations it is convenient to choose the set $\lambda^\mu = \{\mathcal{A}, t_a, \Phi, \tau_0, \tau_1\}$ where $\mathcal{A}$ is the amplitude parameter, t_a and Φ are the time of arrival of the signal and its phase at the time of arrival, respectively, and τ_0 and τ_1 are the Newtonian and the post-Newtonian coalescence times. For noise in realistic detectors, such as LIGO, the elements of the Fisher information matrix cannot be expressed in a closed form and, for the set of parameters employed, it is not useful to explicitly write down the covariance matrix in terms of the various integrals since the errors and covariances do not have any dependence on the parameters. We thus evaluate the information matrix numerically and then take its inverse to obtain the covariance matrix. Instead of dealing with the covariance matrix C it more instructive to work with the matrix of standard deviations and correlation coefficients D which is related to the former by

$$D_{\mu\nu} = \begin{cases} \sqrt{C_{\mu\nu}} & \text{if } \mu = \nu, \\ C_{\mu\nu}/(\sigma_\mu \sigma_\nu) & \text{if } \mu \neq \nu, \end{cases} \tag{4.2}$$

where $\sigma_\mu = D_{\mu\mu}$ is the 1σ uncertainty in the parameter λ_μ. The off-diagonal elements of D take on values in the range $[-1, 1]$, indicating how two different parameters are correlated: For $\mu \neq \nu$, $D_{\mu\nu} = 1$ indicates that the two are perfectly correlated, $D_{\mu\nu} = -1$ means that they are perfectly anticorrelated, and $D_{\mu\nu} = 0$ implies that they are uncorrelated. Since the information matrix is block diagonal, the amplitude parameter is totally uncorrelated with the rest and thus an error in the measurement of $\mathcal{A}$ will not reflect itself as an error in the estimation of the other parameters and vice versa. In contrast, as we shall see below, Newtonian chirp time is strongly anticorrelated to post-Newtonian chirp time, which implies that if in a given experiment τ_0 happens to be estimated larger than its true value, then it is more likely that τ_1 will be estimated to be lower than its actual value. Such correlations are useful as far as detection is concerned since they tend to reduce the number of templates needed in filtering a given signal. On the other hand, strong correlations between the parameters increase the volume in the parameter space to which an event can be associated at a given confidence level. It seems to be in general true that a given set of parameters do not satisfy the twin properties of having small covariances and reducing the effective dimension of the manifold for the purpose of filtering. We elaborate on this point below.

Given a region in a parameter space, it is useful to know the proper volume (as defined by the metric) of the manifold corresponding to the said region. In choosing a discrete set of filters for the detection problem one has to decide upon the maximum allowable drop in the correlation due to the finite spacing. Once this is fixed, the number of filters can be determined from the total volume of the manifold. For the detection problem it is beneficial to have a small volume, whereas if the waveform is parametrized in a way such that the manifold corresponding to it covers a large volume, then one can determine the parameters to a greater accuracy. As a simple example let us consider a two-dimensional toy model $\boldsymbol{\lambda} = \{\lambda_1, \lambda_2\}$. We compare different signal manifolds each corresponding to a different parametrizations of the waveform. We assume the covariance matrix and its inverse, the Fisher information matrix, to be

$$C_{\mu\nu} = \begin{pmatrix} \sigma_{11} & \sigma_{12} \\ \sigma_{12} & \sigma_{22} \end{pmatrix} \quad \text{and} \quad \Gamma_{\mu\nu} = \begin{pmatrix} \gamma_{11} & \gamma_{12} \\ \gamma_{12} & \gamma_{22} \end{pmatrix} = \frac{1}{(\sigma_{11}\sigma_{22} - \sigma_{12}^2)} \begin{pmatrix} \sigma_{22} & -\sigma_{12} \\ -\sigma_{12} & \sigma_{11} \end{pmatrix}. \tag{4.3}$$

The volume of the manifold corresponding to a region $\mathcal{K}$ of the parameter space is given as

$$V_{\mathcal{K}} = \int_{\mathcal{K}} \gamma_{11}\gamma_{22} \left[1 - \frac{\gamma_{12}^2}{\gamma_{11}\gamma_{22}}\right] d\lambda_1 d\lambda_2 = \int_{\mathcal{K}} \gamma_{11}\gamma_{22} \left[1 - \epsilon\right] d\lambda_1 d\lambda_2, \tag{4.4}$$

where $\epsilon = \gamma_{12}^2/(\gamma_{11}\gamma_{22})$ is the correlation coefficient. It can be clearly seen that if for a given set of values of the variances the correlation coefficient is small, then the volume of the manifold is maximal. Since the parameters τ_0 and τ_1 are highly anticorrelated, the proper volume corresponding to the region reduces to zero, showing that the effective dimensionality of the manifold is less.

Though, in principle, the variances and covariances are independent of the chirp time, in reality there arises an indirect dependence since one terminates a template at a frequency $f = 1/(6^{3/2}\pi M)$ (where M is the total mass of the binary) corresponding to the plunge radius at $a = 6M$ [20]. Therefore, larger mass binaries are tracked over a smaller bandwidth so much so that there is less frequency band to distinguish between two chirps of large, but different, total mass. Consequently, at a given SNR the error in the estimation of chirp times is larger for greater mass binaries. This is reflected by the fact that the integrals in Eq. (3.17) are somewhat sensitive to the value of the upper cutoff. (This also explains why the errors in the estimation of the chirp and reduced masses are larger for greater mass binaries [23,20].) In the following we assume that the noise power spectral density is that corresponding to the initial LIGO for which a fit has been provided by Finn and Chernoff [23]. For a SNR of 10 the matrix D is given by

$$D_{\mu\nu} = \begin{pmatrix} 1.0 & 0 & 0 & 0 \\ & 8.37 & 0.999 & -0.999 \\ & & 3.16 & -0.998 \\ & & & 8.4 \end{pmatrix}, \tag{4.5}$$

for the Newtonian signal, and by

$$D_{\mu\nu} = \begin{pmatrix} 1.0 & 0 & 0 & 0 & 0 \\ & 20.4 & 0.997 & -0.972 & 0.911 \\ & & 6.7 & -0.954 & 0.881 \\ & & & 45.1 & -0.982 \\ & & & & 25.98 \end{pmatrix}, \tag{4.6}$$

for the first post-Newtonian corrected signal. While computing variances and covariances the integrals in Eq. (3.19) are evaluated by choosing a finite upper limit of 1 kHz. In the above matrices the entries are arranged in the order $\{\mathcal{A}, t_a, \Phi, \tau_0\}$ in the Newtonian case, $\{\mathcal{A}, t_a, \Phi, \tau_0, \tau_1\}$ in the post-Newtonian case, off-diagonal elements are dimensionless correlation coefficients, and, where appropriate, diagonal elements are in ms. The values quoted in the case of the Newtonian waveform are consistent with those obtained using a different set of parameters by Finn and Chernoff [23]. In order to demonstrate the effect of the plunge cutoff we have, in Fig. 3, plotted σ's, at a SNR of 10, as a function of the upper

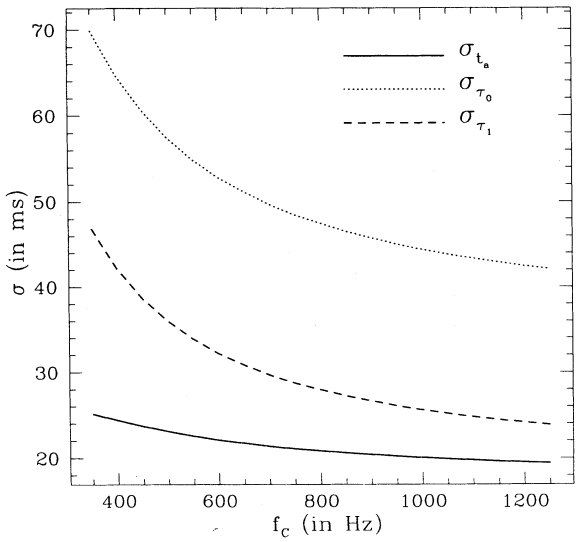

FIG. 3. Dependence of the errors in the estimation of the parameters of the post-Newtonian waveform on the upper cutoff frequency. The SNR is kept fixed at a value of 10.

frequency cutoff f_c for Newtonian and post-Newtonian chirp times and the instant of coalescence, t_C. We see that σ is larger for higher mass binaries, but this is because we have fixed the SNR. However, if we consider binaries of different total masses, all located at the same distance, then a more massive binary produces a stronger SNR so that in reality it may be possible to determine its parameters more accurately than that of a lighter binary. In Fig. 4 we have plotted σ's for binaries, all located at the same distance as a function of the total mass. We

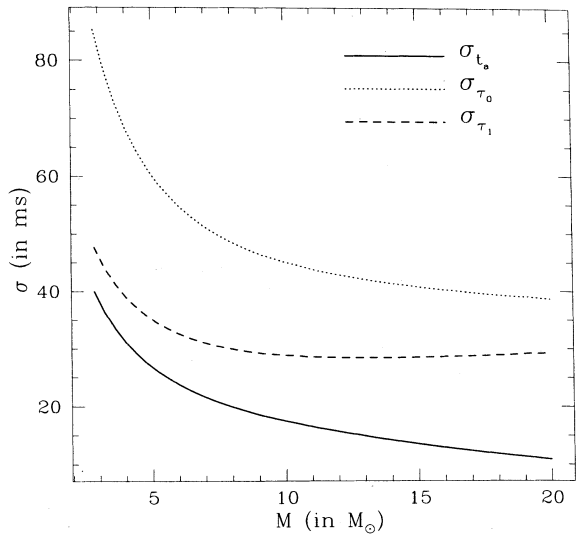

FIG. 4. Dependence of the errors in the estimation of the parameters of the post-Newtonian waveform on the total mass of the binary keeping the distance to the binary fixed. The waveforms are cutoff at frequencies corresponding to the onset of the plunge orbit and the SNR is normalized at a value of 10 for a 1.4 $M_\odot$-10 $M_\odot$ binary.

fix one of the masses at a value of 1.4 $M_\odot$ and vary the other from 1.4 $M_\odot$ to 10 $M_\odot$. In computing the σ's plotted in this figure we have terminated the waveform at the plunge orbit and normalized the SNR of a $10M_\odot$-$1.4M_\odot$ binary system to 10. As a function of M the uncertainties in τ_0 and τ_1 initially fall off since the increase in the SNR for larger mass binaries more than compensates for the drop in the upper frequency cutoff. However, for M larger than a certain M_0 the increase in the SNR is not good enough to compensate for the drop in f_c, so much so that the uncertainties in τ_0 and τ_1 increase beyond M_0. The parameter t_a, however, falls off monotonically.

B. Monte Carlo estimation of parameters

In this section we present the first in a series of efforts to compute the covariance matrix of errors through numerical simulations for a coalescing binary waveform at various post-Newtonian orders. Analytical computation of the covariance matrix, as in the previous section, gives us an idea of the covariances and variances but, as we shall see in this section, at low SNR's it grossly underestimates the errors. Quite apart from the fact that the assumptions made in deriving the covariance matrix might be invalid at low SNR's, in a realistic detection and data analysis, other problems, such as discreteness of the lattice of templates, finite sampling of the data, etc., do occur. It therefore seems necessary to check the analytical calculations using numerical simulations to gain further insight into the accuracy at which physical parameters can be measured. This section is divided into several parts: In the first part we highlight different aspects of the simulation, in the second part we briefly discuss the choice of templates for the simulation, in the third we elaborate on the Monte Carlo method that we have adopted to carry out our simulations, and in the fourth we discuss problems that arise in a numerical simulation. The results of our study are discussed in the next section.

1. Parameters of the simulation

Let $s(t)$ be a signal of strength $\mathcal{A}$ characterized by a set of parameters $\hat{\boldsymbol{\lambda}}$:

$$s(t;\hat{\boldsymbol{\lambda}}) = \mathcal{A}h(t;\hat{\boldsymbol{\lambda}}), \quad \langle h,h\rangle = 1. \tag{4.7}$$

In data analysis problems one considers a discrete version $\{s^k | k = 0,\ldots,N-1\}$ of the waveform $s(t)$ sampled at uniform intervals in t:

$$s^k \equiv s(k\Delta); \quad k = 0,\ldots,N-1, \tag{4.8}$$

where Δ denotes the constant interval between consecutive samples and N is the total number of samples. The sampled output x^k of the detector consists of the samples of the noise plus the signal:

$$x^k = n^k + s^k. \tag{4.9}$$

The *sampling rate* $f_s = \Delta^{-1}$ (also referred to as the *sampling frequency*) is the number of samples per unit time interval. In a data analysis problem the sampling frequency is determined by the signal bandwidth. If B is the signal bandwidth, i.e., if the Fourier transform of the signal is only nonzero over a certain interval B, then it is sufficient to sample at a rate $f_s = 2B$. In our case there is a lower limit in the frequency response of the detector since the detector noise gets very large below a seismic cutoff at about 10–40 Hz. As mentioned in the last section there is also an upper limit in frequency up to which a chirp signal is tracked since one does not accurately know the waveform beyond the last stable circular orbit of the binary. This corresponds to gravitational wave frequency $f_c = 1/(6^{3/2}\pi M)$. For a neutron-star–neutron-star (NS-NS) binary $f_c \sim 1525$ Hz while for a NS–black-hole (of 10 $M_\odot$) (NS-BH) binary $f_c \sim 375$ Hz. Because of constraints arising out of limited computational power, we terminate waveforms at 750 Hz even when f_c is larger than 1000 Hz. Such a shutoff is not expected to cause any spurious results since, even in the case of least massive binaries of NS-NS, which we consider in this study, more than 99% of the "energy" is extracted by the time the signal reaches 750 Hz. We have carried out simulations with two types of upper cutoff: (1) one in which all templates, irrespective of their total mass, are shut off beyond 750 Hz; (2) a second in which the upper frequency cutoff is chosen to be 750 Hz or f_c, whichever is lower. Consistent with these cutoffs the sampling rate is always taken to be 2 kHz. (We have carried out simulations with higher sampling rates and found no particular advantage in doing so; nor did we find appreciable changes in our results.)

In all our simulations, as in the previous section, we take the detector noise power spectral density S to be that corresponding to the initial LIGO [23]. For the purpose of simulations we need to generate noise corresponding to such a power spectrum. This is achieved by the following three steps.

(1) Generate Gaussian white noise n'^k with zero mean and unit variance:

$$\overline{n'^k} = 0, \quad \overline{n'^k n'^l} = \delta^{kl},$$

where an overbar denotes average over an ensemble.

(2) Compute its Fourier transform

$$\tilde{n}'^k \equiv \frac{1}{\sqrt{N}} \sum_{l=0}^{N-1} n'^l \exp(2\pi i k l/N).$$

(3) Multiply the Fourier components by the square root of the power spectral density:

$$\tilde{n}^k = \sqrt{S^k}\tilde{n}'^k.$$

The resultant random process has the requisite power spectrum. In the above, the second step can be eliminated since the Fourier transform of a Gaussian random process is again a Gaussian, but with a different variance. In other words we generate the noise directly in the Fourier domain. The simulated detector output, in the presence of a signal s^k, in the Fourier domain is given by

$$\tilde{x}^k = \tilde{n}^k + \tilde{s}^k, \tag{4.10}$$

where $\tilde{s}^k$ is the discrete Fourier transform of the signal.

2. Choice of templates

To filter a Newtonian signal we employ the set of parameters $\{t_a, \Phi, \tau_0\}$ and to filter a post-Newtonian signal we employ the set $\{t_a, \Phi, \tau_0, \tau_1\}$. Templates need not explicitly be constructed for the time of arrival since computation of the scalar product in the Fourier domain [and the availability of fast Fourier transform (FFT) algorithms] takes care of the time of arrival in essentially one computation ($N \ln_2 N$ operations as opposed to N^2 operations, where N is the number of data points). Moreover, there exists a two-dimensional basis for the phase parameter which allows the computation of the best correlation with the aid of just two filters. Consequently, the parameter space is essentially one dimensional in the case of Newtonian signals and two dimensional in the case of post-Newtonian signals. (However, as shown in Sec. III C it is to be noted that for the purpose of detection the effective dimensionality of the parameter space, even with the inclusion of second post-Newtonian corrections, is only one dimensional.) We adopt the method described in Sathyaprakash and Dhurandhar [13] to determine the templates needed for chirp times. As described in [13,29] filters uniformly spaced in τ_0 and τ_1 cover the parameter space efficiently.

3. Monte Carlo method

In order to compute variances and covariances numerically, we employ the Monte Carlo method. The basic idea here is to mimic detection and estimation on a computer by performing a very large number of simulations so as to minimize the uncertainties induced by noise fluctuations. In our simulations we generate a number of detector outputs $\{\mathbf{x}^k\}$ each corresponding to a definite signal $\mathbf{s}(\hat{\boldsymbol{\lambda}})$ of a certain strength, but corresponding to different realizations of the random process $\{\mathbf{n}^k\}$. Computation of the covariance matrix involves filtering each of these detector outputs through an *a priori* chosen set (or lattice) of templates $\{q(t;{}_t\boldsymbol{\lambda}_k)|k = 1, \ldots, n_f\}$, where n_f denotes the number of templates. The templates of the lattice each have a distinct set of values of the *test* parameters ${}_t\boldsymbol{\lambda}_k$ and together they span a sufficiently large volume in the parameter space. The simulated detector output is correlated with each member of the lattice to obtain the corresponding filtered output $C({}_t\boldsymbol{\lambda}_k)$:

$$C({}_t\boldsymbol{\lambda}_k) = \langle x, q({}_t\boldsymbol{\lambda}_k)\rangle\,. \tag{4.11}$$

For a given realization of noise a particular template obtains the largest correlation and its parameters are the *measured* values ${}_m\boldsymbol{\lambda}$ of the signal parameters. Thus, the measured values of the parameters are defined by

$$\max_k C({}_t\boldsymbol{\lambda}_k) = C({}_m\boldsymbol{\lambda}). \tag{4.12}$$

The measured values, being specific to a particular realization of noise, are random variables. Their average provides an estimation ${}_e\boldsymbol{\lambda}$ of the true parameter values and their variance is a measure of the error $\sigma_{\boldsymbol{\lambda}}$ in the estimation:

$${}_e\boldsymbol{\lambda} = \overline{{}_m\boldsymbol{\lambda}}, \qquad \sigma_{\boldsymbol{\lambda}}^2 = \overline{\left({}_m\boldsymbol{\lambda} - \overline{{}_m\boldsymbol{\lambda}}\right)^2}, \qquad D^{\mu\nu} = \frac{\overline{{}_m\lambda^\mu \, {}_m\lambda^\nu}}{\sigma_\mu \sigma_\nu}, \quad (\mu \neq \nu), \tag{4.13}$$

where $D_{\mu\nu}$ are the correlation coefficients between parameters λ_μ and λ_ν. In order to accurately determine $\sigma_{\boldsymbol{\lambda}}$ a large number of simulations would be needed. If the measured values ${}_m\boldsymbol{\lambda}$ obey Gaussian statistics, then after N_t trials the variance is determined to a relative accuracy $1/\sqrt{N_t}$ and estimated values can differ from their true values by $\sigma_{\boldsymbol{\lambda}}/\sqrt{N_t}$. We have performed in excess of 5000 trials, for each input signal, and thus our results are accurate to better than 1 part in 70. Even more crucial than the number of simulations is the number of templates used and their range in the parameter space. We discuss these and other related issues next.

The actual templates chosen, say, for the parameter τ_0, in a given "experiment" depend on the true parameters of the signal, the number of noise realizations employed, and the expected value of the error. Let us suppose we have a first guess of the error in τ_0, say, σ_{τ_0}. Then, we choose 51 uniformly spaced filters around $\hat{\tau}_0$ (where $\hat{\tau}_0$ is the signal chirp time) such that

$${}_t\tau_0 \in [\hat{\tau}_0 - 5\sigma_{\tau_0}, \hat{\tau}_0 + 5\sigma_{\tau_0}]. \tag{4.14}$$

This implies that we are covering a 5σ width in τ_0 at a resolution of $\sigma_\tau/5$. The probability that a template between 4σ and 5σ from the true signal "clicks" being $\sim 6 \times 10^{-5}$, we are on safe grounds since, in a given simulation, we consider no more than 5000 trials. (In comparison, the probability that a template between 3σ and 4σ clicks is 2.2×10^{-3}, corresponding to an expected 13 events in 5000 trials.) For a post-Newtonian signal, which in effect needs to be spanned by a two-dimensional lattice of filters, the above choice of templates implies a requirement of 2601×2 filters in all. Here a factor of 2 arises because for each filter in the τ_0-τ_1 space we will need two templates corresponding to the two independent values of the phase Φ: 0 and $\pi/2$. In the case of a Newtonian signal, the lattice being one dimensional, one can afford a much higher resolution and range. Even with the aid of a mere 201 templates we can probe at a $\sigma/10$ resolution with a 10σ range.

We start off a simulation with the pretension that there is no knowledge of what the $\sigma_{\boldsymbol{\lambda}}$'s are. Thus, we choose as our first trial a very large $\sigma_{\boldsymbol{\lambda}}$ and lay the lattice of templates. With this lattice we perform a test run of 400 trials and examine the distribution of the measured values. If the distribution is not, as expected, a Gaussian, then we alter $\sigma_{\boldsymbol{\lambda}}$: We decrease it if the distribution is too narrow and increase it if the distribution is too wide and does not show the expected falloff. In particular, we make sure that the templates at the boundary of the chosen range do not click even once and the skewness of the distribution is negligible. When for a certain $\sigma_{\boldsymbol{\lambda}}$ a rough Gaussian distribution is observed, then we carry out a simulation with a larger number of trials (typically 5000). We subject the measured values in this larger simulation to the very same tests described above. We only consider for further analysis such simulations which "pass" the above tests and determine the estimates, variances, and covariances of the parameters using the measured values, with the aid of Eq. (4.13).

4. Numerical errors and remedies

There are several sources of numerical errors that tend to bias the results of a simulation unless proper care is exercised to rectify them. In this section we point out the most important ones and show how they can be taken care of. Because of memory restrictions, the present version of our codes works with single precision except the FFT, which is implemented in double precision. In future implementations we plan to carry out all computations in double precision. This will possibly reduce some of the numerical noise that occurs, especially at high SNR's, in the present simulations.

(1) *Orthonormality of filters:* For the sake of simplicity it is essential that the filters are normalized in the sense that their scalar product is equal to unity: $\langle q, q\rangle = 1$. A waveform is normalized numerically using the discrete version of the scalar product; i.e., the normalization constant is chosen to be [cf. Eq. (2.16)]

$$\mathcal{N} = \frac{1}{\sum_{k=0}^{N-1} S_k^{-1} \, |\tilde{q}^k|^2}. \tag{4.15}$$

As mentioned earlier we use a two-dimensional basis of filters for the phase parameter. Choosing the two filters to be orthogonal to each other makes the maximization over the phase easier. However, here care must be exercised. Two filters $q(t; t_a, \tau_0, \tau_1, \Phi = 0)$ and $q(t; t_a, \tau_0, \tau_1, \Phi = \pi/2)$ are apparently orthogonal to each other. The numerically computed 'angle' between the two filters, chosen in this manner, often turns out to be greater than $\sim 10^{-2}$ rad. Consequently, one obtains erroneous correlations. In order to circumvent this problem we first generate two filters that are roughly orthogonal to each other, as above, and then use the Gram-Schmidt method to orthogonalize the two vectors. If an explicit numerical orthogonalization such as this is *not* implemented, then the measured values of the various parameters show spurious oscillations in their distribution and the estimated values of the parameters tend to get biased.

(2) *Correlation function:* The scalar product of two normalized templates $q(t; {}_t\boldsymbol{\lambda})$ and $q(t; {}_t\boldsymbol{\lambda}')$ is given by

$$C({}_t\lambda_\mu, {}_t\lambda'_\nu) = \left\langle q(t; {}_t\lambda_\mu), q(t; {}_t\lambda'_\nu)\right\rangle, \quad \left\langle q(t; {}_t\boldsymbol{\lambda}), q(t; {}_t\boldsymbol{\lambda})\right\rangle = \left\langle q(t; {}_t\boldsymbol{\lambda}'), q(t; {}_t\boldsymbol{\lambda}')\right\rangle = 1, \tag{4.16}$$

where we have indicated the dependence of the scalar product on the various parameters by explicitly writing down the parameter subscripts. Let us fix the parameters of one of the templates, say, ${}_t\boldsymbol{\lambda}$, and vary the parameters of the other template. Of particular interest is the behavior of C maximized over all but one of the parameters, say, λ_{ν_0}:

$$C_{\max}({}_t\lambda_\mu, {}_t\lambda'_{\nu_0}) = \max_{\substack{{}_t\lambda'_\nu \\ \nu\neq\nu_0}} C({}_t\lambda_\mu, {}_t\lambda'_\nu). \tag{4.17}$$

$C_{\max}$ is expected to drop monotonically as $|\lambda_{\nu_0} - \lambda'_{\nu_0}|$ increases. However, we have observed departures from such a behavior possibly arising out of numerical noise. Such a behavior causes bias in the estimation of parameters, and consequently in the determination of their covariances, especially at high SNR's. We have found no remedy to this problem and some of our results at high SNR's may have biases introduced by this effect. (Sampling the templates at a higher rate did not help in curing this problem.)

(3) *Grid effects:* The parameters of a signal chosen for the purpose of simulation and detection can in principle be anything and in particular it need not correspond to any of the templates of the lattice. However, in practice we find that whenever the signal parameters do not correspond to a member of the lattice the resultant simulation has a bimodal distribution of the measured values. This is, of course, expected since a signal not on the grid is picked up by two nearest templates along each direction in the parameter space. Sometimes we do find that the peaks corresponding to the bimodal distribution do not belong to the nearest neighbor filters but slightly away. This is related to the fact that the correlation function maximized over the time of arrival and the phase of the signal fall off much too slowly along the τ_0-τ_1 direction and a small deviation from a monotonic fall can cause biases. (Such biases would be present in the case when a signal corresponds to one of the grid points though the magnitude of the effect would be lower.) In order to avoid this problem, and the consequent shifts in the estimation of parameters and errors in the determination of variances and covariances, we always choose the parameters of the signal to be that corresponding to some template.

(4) *Upper frequency cutoff and its effect on parameter estimation:* The Fisher information matrix computed using the stationary phase approximation in Sec. III does not include the effect of truncating the waveform at $a = 6M$, the plunge cutoff. As mentioned before, we have carried out simulations both with and without incorporating the upper cutoff. As the covariance matrix incorporating the upper cutoff is not available we have been able to compare the Monte Carlo results with the covariance matrix only for the latter case, where the cutoff is held fixed at 750 Hz. If we incorporate the upper cutoff into the Monte Carlo simulations, the errors in the parameters are reduced drastically. The effect of the upper cutoff is expected to be more important for the higher mass binaries such as the ones we have considered. The ambiguity function, in this case, no longer remains independent of the point on the manifold. In other words, the correlation between two chirps depends not only on the difference between the parameters of the signals, but also on the absolute values of the parameters. The correlation surface also ceases to be symmetric; i.e., the correlation between two chirps also depends on the sign of $\delta\lambda$, where $\delta\lambda$ is the difference in the values of the parameters. As the computational power required for carrying out simulations for lower mass binaries is not available to us the simulations have been restricted to NS-BH binaries, where the effect of the upper cutoff is important.

(5) *Boundary effects:* For the purpose of simulations a grid of filters has to be set up "around" the signal. The grid must be large enough so that the measured parameters do not overshoot the boundary of the grid. This causes a problem as every value in the $\{\tau_0, \tau_1\}$ plane does not lead to a meaningful value for the masses of the binary system. This does not, however, prevent us from constructing a waveform with such a value for $\{\tau_0, \tau_1\}$ even though the signal in general does not correspond to any "real" binary system. This is valid, and even necessary, if we are to compare the numerical results with the covariance matrix.

(6) *Incorporating the cutoff in the presence of boundary effects:* If we wish to incorporate the effects of the upper cutoff in simulations, then we run into a serious problem, as we would have to know the total mass of the binary in order to compute the upper cutoff. For an arbitrary $\{\tau_0, \tau_1\}$ we can end up with negative and even complex values of the total mass and hence the upper cutoff at $a = 6M$ is not meaningful. Thus, we cannot even construct a waveform for an arbitrary combination of $\{\tau_0, \tau_1\}$. Therefore, in such cases, we restrict ourselves to simulations where the grid lies entirely within valid limits for $\{\tau_0, \tau_1\}$.

C. Results and discussion

Our primary objective is to measure the variances and covariances following the method described in Sec. IV B 3 and study their departure from that predicted by analytical means (cf. Sec. IV A). We have carried out simulations for several values of the masses of the binary and in each case the signal strength (which is a measure of the SNR) is varied in the range 10–40. However, since the variances and covariances are independent of the absolute values of the parameters, for the parameter set that we employ, results are only quoted corresponding to a typical binary system. (See Sec. IV A for a discussion of the covariance matrix.) Similar results are obtained in other cases too. We use two sets of parameters to describe our results. Monte Carlo simulations allow us to directly measure the amplitude, the time of arrival, the phase at the time of arrival, and the chirp time(s). This is the set $\{\mathcal{A}, t_a, \Phi, \tau_0, \tau_1\}$.

As we shall see below, the instant of coalescence can be measured much more accurately than the time of arrival. As a consequence of this, the direction to the source can be determined at a *much greater accuracy* by employing t_C as a parameter instead of t_a [30]. Thus, we also quote estimates and errors for the parameter t_C. Since the error

in the estimation of the phase is quite large, even at high SNR's, we ignore it in our discussions.

We first deal with the Newtonian signal and highlight different aspects of the simulation and discuss the results at length. We then consider the first post-Newtonian corrected signal.

1. *Newtonian signal*

In the case of Newtonian signals the parameter space is effectively one dimensional and, as mentioned earlier, in this case the lattice of templates covers a 10σ range of the parameters at a resolution of $\sigma/10$ centered around the true parameters of the signal.

In Fig. 5 we have shown the error $\sigma_{\boldsymbol{\lambda}}$ in the estimation of parameters t_a, τ_0, and t_C, as a function of the SNR, deduced using the covariance matrix as solid lines and computed using Monte Carlo simulations as dotted lines. The curve corresponding to the covariance matrix is obtained using an upper frequency cutoff $f_c = 750$ Hz consistent with that used in our simulations. The error bars in the estimation of $\sigma_{\boldsymbol{\lambda}}$'s are obtained using four simulations, each with 5000 trials. At low SNR's, $\sigma_{\boldsymbol{\lambda}}$'s have a larger uncertainty, as expected, and for $\rho > 30$ this uncertainty is negligible, and sometimes smaller than the thickness of the curves, except in the case of σ_{t_C} (see below, for a possible explanation).

At low SNR's (10–15) there is a large departure of the various $\sigma_{\boldsymbol{\lambda}}$'s from that inferred using the covariance matrix. At a SNR ~ 17 the two curves merge (except in the case of σ_{t_C}), indicating the validity of the covariance matrix results for this and higher SNR's. Interestingly, the agreement between Monte Carlo simulation results and those obtained using the covariance matrix is reached roughly at the same SNR irrespective of the parameter in question.

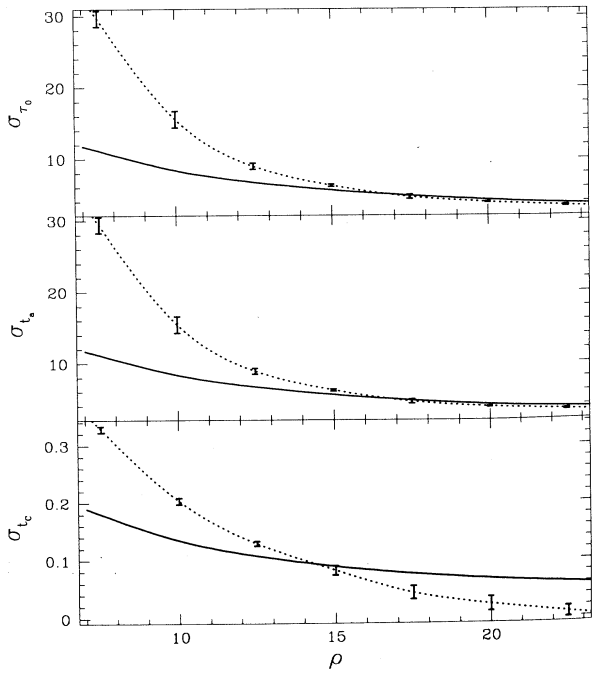

FIG. 5. Dependence of the errors in the estimation of parameters of the *Newtonian* waveform, i.e., $\{\sigma_{\tau_0}, \sigma_{t_a}, \sigma_{t_C}\}$, as a function of the SNR. The solid line represents the analytically computed errors whereas the dotted line represents the errors obtained through Monte Carlo simulations.

We note that in spite of the fact that the time of arrival and the chirp time having large errors, the instant coalescence can be estimated very accurately, an order of magnitude better than either. What is puzzling, however, is that, in the case of t_C, the Monte Carlo curve drops below the covariance matrix curve above a SNR of 15 and the two curves do not seem to converge to one another even at very high SNR's. Coincident with the crossover of the two curves, the error in the estimation of σ_{t_C} increases, contrary to what happens for the other parameters, signaling that there is a large fluctuation in the estimation of σ_{t_C}. This behavior, we guess, is an artifact of the low value of the sampling rate and template spacing. Of course, our sampling rate is sufficiently high to respect the sampling theorem. However, since t_C is determined to an accuracy an order of magnitude better than either t_a or τ_0, a much higher resolution in template spacing would be needed for determining the error in the instant of coalescence than that used for estimating the errors in the time of arrival or the chirp time(s). Testing this claim, unfortunately, is beyond the computer resources at our disposal since we would need a sampling rate of about 10 kHz with a filter spacing 10^{-4} s. We hope to be able to resolve this issue in the course of time. Nevertheless, the fact that the error in the estimation of σ_{t_C} first decreases with the SNR and increases only after the two curves crossover hints at the above possibility as a cause for this anomalous behavior. This effect is also observed in the case of a post-Newtonian signal.

In Table I we have given the actual signal parameters $\hat{\boldsymbol{\lambda}}$, estimated values of the parameters ${}_e\boldsymbol{\lambda}$ [cf. Eq. (4.13)], and the corresponding errors in their estimation, $\sigma_{\boldsymbol{\lambda}}$, for several values of the SNR. Errors inferred from the covariance matrix can be read off from Fig. 5. The estimated values are different from the true values, some of them being overestimated and some others underestimated. However, the deviations are often larger than what we expect. In a simulation that uses N_t trials the estimated parameters ${}_e\boldsymbol{\lambda}$, assuming a Gaussian distribution for the measured parameters ${}_m\boldsymbol{\lambda}$, can be different from the true values by $\sigma_{\boldsymbol{\lambda}}/\sqrt{N_t}$. (In contrast, the measured values ${}_m\boldsymbol{\lambda}$ can differ from their true values by $\sigma_{\boldsymbol{\lambda}}$ or more.) However, we often obtain a slightly larger deviation

$$\lesssim 2\frac{\sigma_{\boldsymbol{\lambda}}}{\sqrt{N_t}} \left| {}_e\boldsymbol{\lambda} - \hat{\boldsymbol{\lambda}} \right| \lesssim 3\frac{\sigma_{\boldsymbol{\lambda}}}{\sqrt{N_t}}, \tag{4.18}$$

and we are unable to resolve this discrepancy. A more concrete test for the simulations is the histogram $n({}_m\boldsymbol{\lambda})$ of the measured parameters, namely, the frequency at which a given test parameter clicks in a simulation. This is shown plotted in Fig. 6 for a SNR of 10. The skewness of the distribution is less than 10^{-2}. These results lend further support to the Monte Carlo simulations. There are visible asymmetries in the distributions of τ_0 and

TABLE I. The estimated value of the parameters and their errors ${}_e\lambda$ (σ_λ) for the Newtonian waveform. The actual values of the parameters taken were $\hat{\tau}_0 = 5558.0$ ms and $\hat{t}_a = 200.0$ ms. Except for the parameter $\mathcal{A}$ all values are quoted in ms.

	$\rho = 7.5$	$\rho = 10.0$	$\rho = 12.5$	$\rho = 15.0$	$\rho = 20.0$
${}_e\tau_0$ (σ_{τ_0})	5557.4 (29.7)	5557.3 (15.6)	5557.6 (9.0)	5557.7 (6.2)	5558.5 (3.9)
${}_et_a$ (σ_{t_a})	200.6 (29.4)	200.7 (15.5)	200.4 (8.9)	200.3 (6.2)	199.5 (3.9)
${}_et_C$ (σ_{t_C})	5758.0 (0.30)	5758.0 (0.20)	5758.0 (0.10)	5758.0 (0.08)	5758 (0.02)
${}_e\mathcal{A}$ ($\sigma_{\mathcal{A}}$)	7.696 (0.96)	10.12 (0.98)	12.582 (0.99)	15.067 (0.99)	20.05 (0.99)

t_a and the asymmetries in the two cases are of opposite sense. This can, of course, be understood from the fact that t_a and τ_0 have a negative correlation coefficient. The histogram of t_C, even at a SNR of 10, has very few nonzero bins. This reflects the fact that it is determined very accurately. We are unable to resolve the central peak in $n(t_C)$ since, as mentioned earlier, the sampling rate and resolution in τ_0 are not good enough to do so.

2. *Post-Newtonian signal*

As opposed to the Newtonian case here we have essentially a two-dimensional lattice of filters corresponding to τ_0 and τ_1. For the purpose estimating variances and covariances we lay a mesh consisting of 2601×2 uniformly spaced filters around the true parameters of the signal. As pointed out in Sec. III B not all filters in the mesh, unlike in the Newtonian case, would correspond to the waveform from a realistic binary but that does not preclude their use in the Monte Carlo simulations. We shall see that the results of our simulations lend further support to the claim that for the purpose of detection, the parameter space need only be one dimensional [29]. The results obtained for the first post-Newtonian signal are qualitatively similar to that of a Newtonian signal and we refer the reader, where appropriate, to the Newtonian case for a more complete discussion.

In Fig. 7 we have shown the error in the estimation of parameters τ_0, τ_1, t_C, and t_a, clockwise from top left, respectively, as a function of SNR. The solid and dotted curves are as in Fig. 5. Here again the upper frequency cutoff is taken to be 750 kHz. Just as in the case of a Newtonian signal here too the results obtained from Monte Carlo simulations are much higher than those obtained by employing the covariance matrix. At a SNR of 10 the Monte Carlo values are more than thrice as much as their corresponding covariance matrix values and at a SNR of 15 the errors are roughly twice that expected

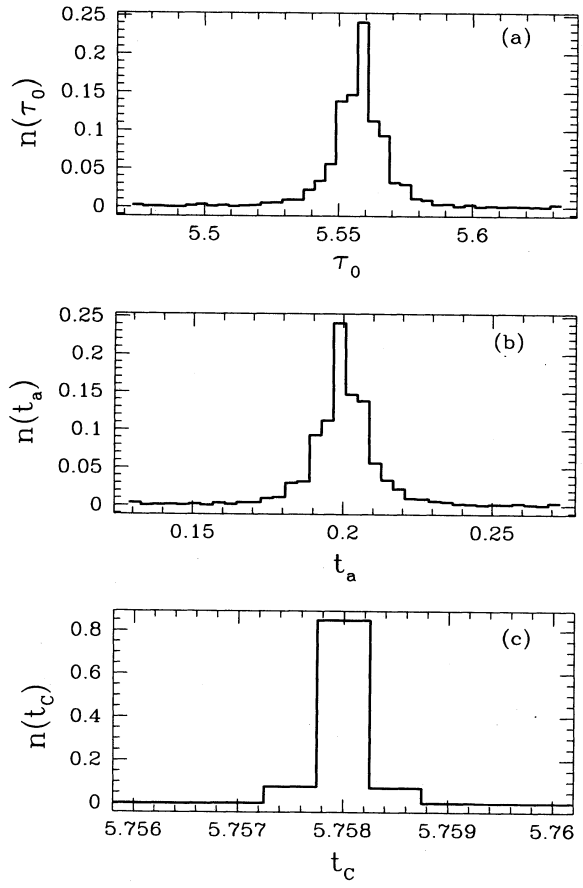

FIG. 6. Distributions of the measured values of the parameters for the case of Newtonian signal. The total number of noise realizations is 5000.

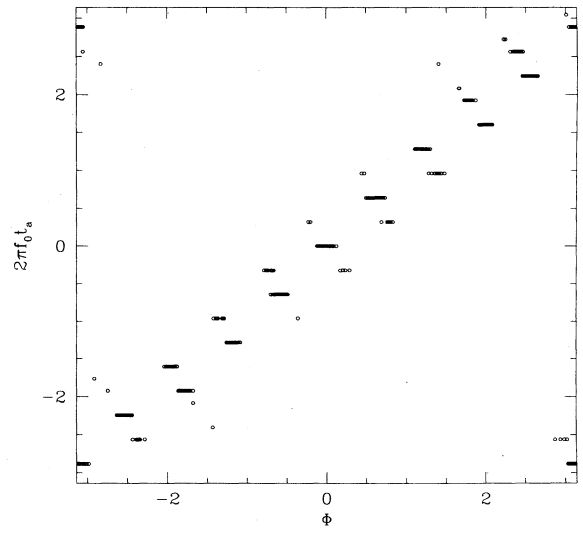

FIG. 7. Dependence of the errors in the estimation of parameters of the post-Newtonian waveform, i.e., $\{\sigma_{\tau_0}, \sigma_{\tau_1}, \sigma_{t_a}, \sigma_{t_C}\}$, as a function of the SNR. The solid line represents the analytically computed errors whereas the dotted line represents the errors obtained through Monte Carlo simulations.

TABLE II. The estimated value of the parameters and the errors in their estimation ${}_e\lambda$ (σ_λ) for the post-Newtonian waveform. The actual values of the parameters taken were $\tau_0 = 5558.0$ ms, $\tau_1 = 684.0$ ms, and $t_a = 300.0$ ms. Except for the parameter $\mathcal{A}$ all values are quoted in ms.

	$\rho = 10.0$	$\rho = 15.0$	$\rho = 20.0$	$\rho = 25.0$	$\rho = 30.0$
${}_e\tau_0$ (σ_{τ_0})	5554.9 (136.1)	5555.9 (64.8)	5557.2 (30.1)	5556.7 (19.3)	5558.7 (13.6)
${}_e\tau_1$ (σ_{τ_1})	685.55 (65)	685.2 (32.6)	684.6 (16.4)	684.8 (10.5)	683.6 (7.2)
${}_et_a$ (σ_{t_a})	301.49 (73.26)	300.88 (33.4)	300.28 (14.5)	300.5 (9.4)	299.7 (6.8)
${}_et_C$ (σ_{t_C})	6.542 (0.54)	6.542 (0.30)	6.542 (0.17)	6.542 (0.10)	6.542 (0.06)
${}_e\mathcal{A}$ ($\sigma_{\mathcal{A}}$)	10.25 (0.97)	15.15 (0.98)	20.11 (.99)	20.1 (0.99)	30.1 (0.99)

from the covariance matrix. In absolute terms, however, the errors are still quite small compared to the actual parameter values: For a NS-NS binary, at a SNR of 10,

$$\frac{\sigma_{\tau_0}}{\tau_0} \sim 2.4\%, \quad \frac{\sigma_{\tau_1}}{\tau_1} \sim 9.4\%. \tag{4.19}$$

At a SNR of 10 the time of arrival can be measured to an accuracy of 72 ms in contrast to a value of 20 ms expected from the covariance matrix. As is well known, with the inclusion of the post-Newtonian terms, the error in the estimation of the time of arrival and Newtonian chirp time increases by about a factor of 2 and 3, respectively [23,20].

As in the Newtonian case here again we see that the Monte Carlo curves approach the corresponding covariance matrix curves at a high SNR, the only difference being that the agreement is reached at a higher SNR $\sim$ 25. For SNR's larger than this the two curves are in perfect agreement with each other. As mentioned earlier, σ_{t_C} shows an anomalous behavior possibly arising out of insufficient resolution in the time of arrival and the chirp times.

In Table II we have listed the true parameters $\hat{\boldsymbol{\lambda}}$, the estimated values ${}_e\boldsymbol{\lambda}$, and the Monte Carlo errors $\sigma_{\boldsymbol{\lambda}}$ for different SNR's. As in the Newtonian case here too the estimated values show a larger departure than expected, from the true values. Histograms of the various measured parameters including t_C are shown in Fig. 8 for a signal strength of 10. The skewness of the distribution is below its standard deviation of $\sqrt{15/N_t}$ [34], indicating the Gaussian nature of the various distributions. Even in the case of a post-Newtonian signal σ_{t_C} is so small that we only have three nonzero bins in $n(t_C)$.

We now turn attention to other, more general, issues arising out of the simulations.

In Sec. III C we have argued, on the basis of the behavior of the noise-free correlation function, that the effective dimensionality of the parameter space for the purpose of detection, even in the case of a post-Newtonian signal, is only one dimensional. The results of our Monte Carlo simulation unambiguously show that this is indeed true even in the presence of noise. We investigated the two-dimensional histogram, which gives the number of occurrences of different templates in the lattice, in a particu-

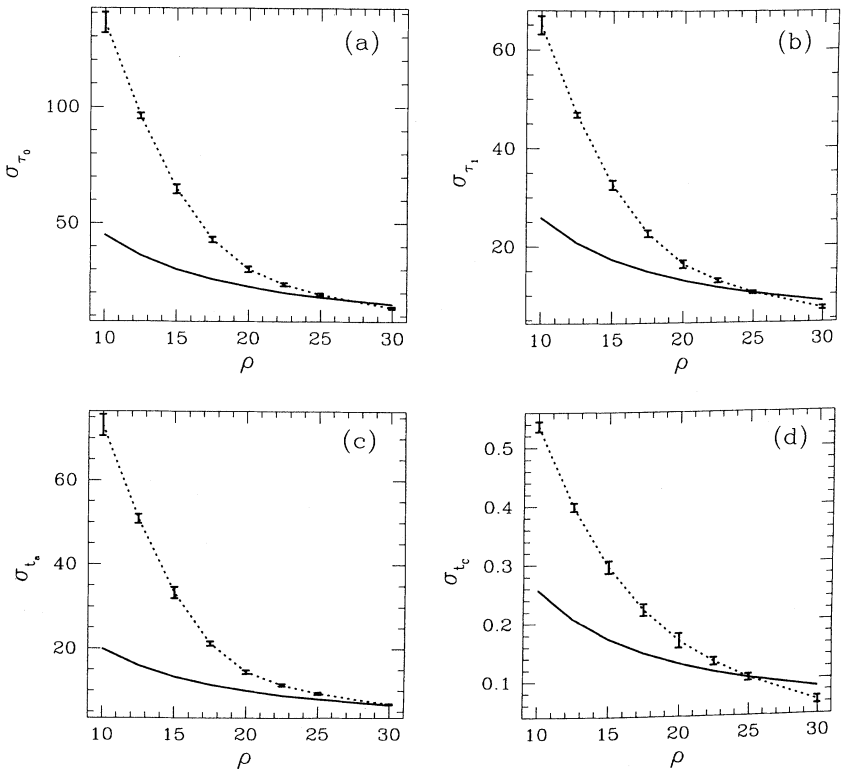

FIG. 8. Distributions of the measured parameters of the post-Newtonian waveform at a SNR of 25. The number of noise realizations is 5000.

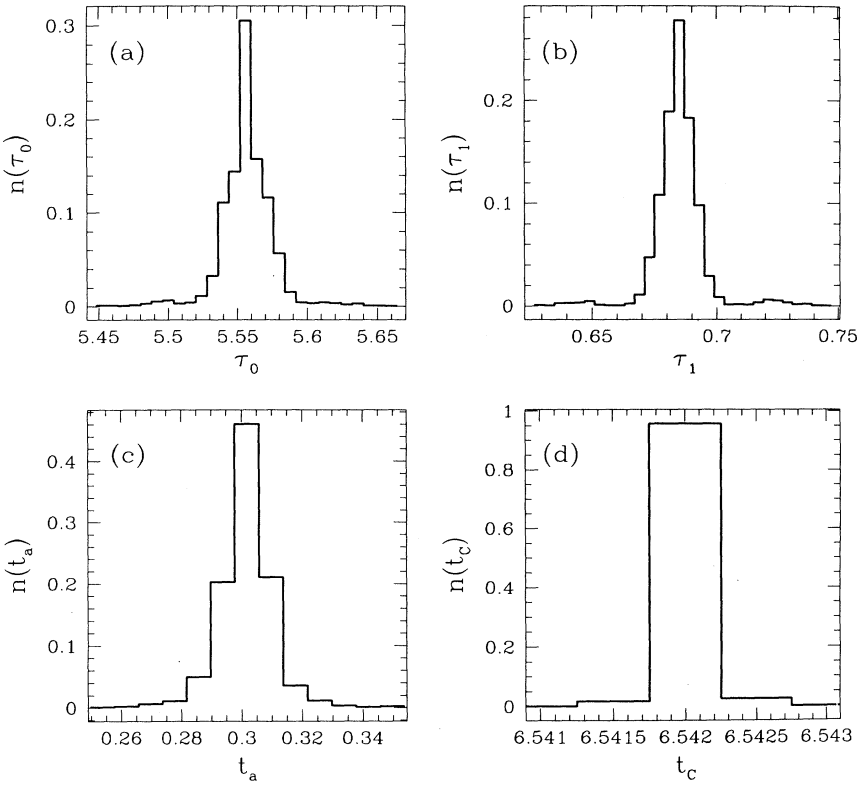

FIG. 9. The histogram of random variable ${}_m\mathcal{A}$ at a SNR of 20. The variance in this parameter is independent of the SNR and is approximately equal to unity.

lar simulation. The templates that "click" are all aligned along the line $\tau_0 + \tau_1 = \text{const}$. In a total of 5000 realizations there is only one instance when a filter outside this region clicks, giving a probability of less than 10^{-3} for a template outside this region to give a maximum. Consequently, it is only necessary to choose a single filter along each of the $\tau_0 + \tau_1 = \text{const}$ lines.

The distribution of the maximum correlation $C_{\max}(\hat{\boldsymbol{\lambda}}, {}_t\boldsymbol{\lambda})$ obtained from different noise realizations needs special mention since it has an inherent bias. In Fig. 9 we have shown the distribution of the maximum correlation taken from one of our simulations corresponding to a SNR of 10. Notice a slight shift of the distribution towards a higher value and this cannot be accommodated within the expected fluctuation in the mean. The measured value of the standard deviation $\sigma_{\mathcal{A}}$ is 0.95. Since the number of simulations is 5000, we expect that the signal strength should differ from the true value of 10 by no more than $\sigma_{\mathcal{A}}/\sqrt{5000} = 0.014$. However, the mean value is 10.26, giving a deviation of 0.26 which is about 20 times larger than that expected. This occurs at all SNR's and for both Newtonian and post-Newtonian signals. This of course does not mean there is a bug in the way we are computing the maximum correlation. In the process of maximization, values greater than the signal strength are favored and consequently the mean of the maximum correlation shows a shift towards a higher value. This suggests that the maximum of the correlation is a biased estimator of the signal strength. Consequently one tends to underestimate the distance to the source.

We find, consistent with the covariance matrix calculation, that the amplitude parameter is uncorrelated with the rest of the parameters; cross-correlation coefficients $D_0\mu$, $\mu \neq 0$ [cf. Eq. (4.2)] inferred from our Monte Carlo simulations are less than $\sim 10^{-6}$.

Finally, it is of interest to note how the phase parameter Φ is correlated with the time of arrival. A plot of ${}_m\Phi$ versus ${}_m t_a$ is shown in Fig. 10. We find that the measured values of the time of arrival and the phase are such that $2\pi f_0\ {}_m t_a = {}_m\Phi$, where f_0 has a value of approximately

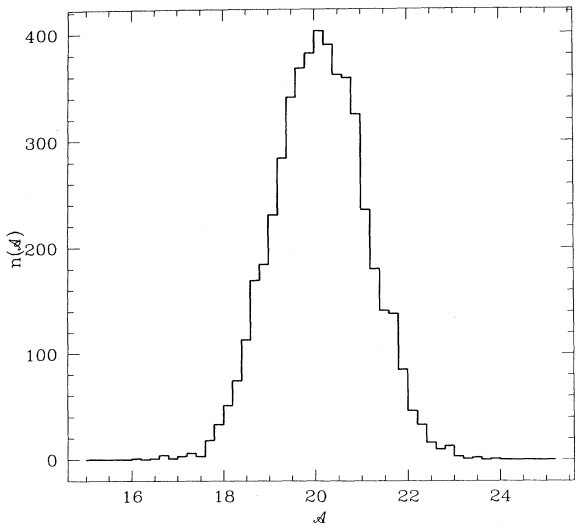

FIG. 10. The correlation between t_a and Φ is illustrated. The phase parameter simply follows the time of arrival parameter.

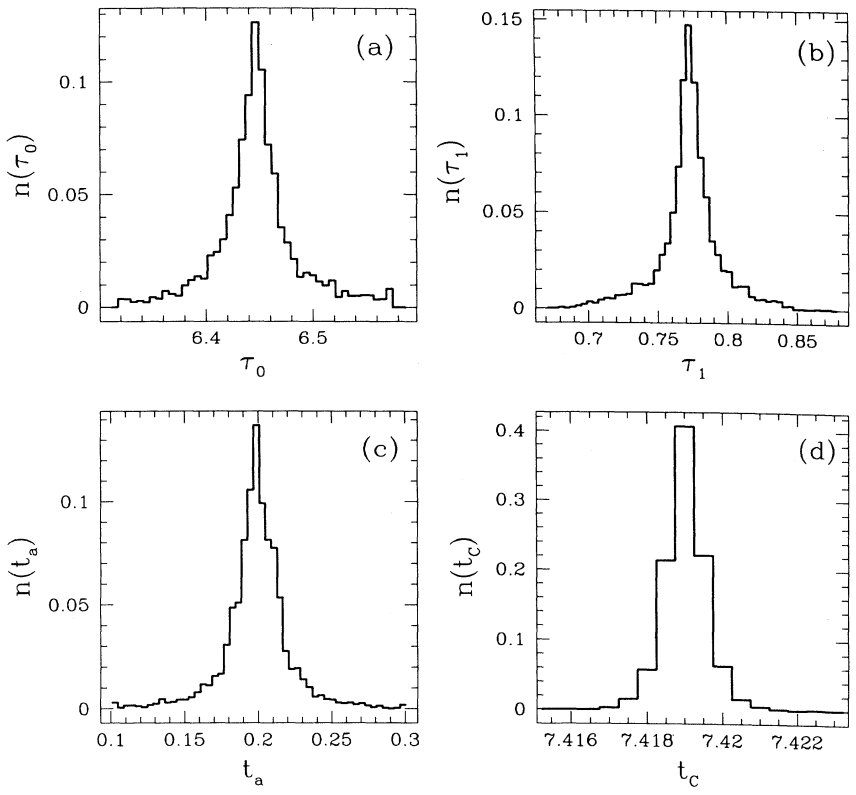

FIG. 11. Distributions for the measured parameters of the post-Newtonian waveform incorporating the effect of the upper cutoff. The errors in the determination of the parameters are much smaller in this case. The total number of noise realizations is 5000.

51 Hz. When the time of arrival shifts by more than a cycle of the signal the phase jumps by a factor 2π, leading to the points seen in the top-left and bottom-right corner of the figure. This makes the estimation of the phase and the error in its estimation pretty involved.

3. *Incorporating the effects of upper cutoff*

As mentioned before, incorporating an upper cutoff at the onset of the plunge has a drastic effect on the estimation of parameters. The incorporation of the upper cutoff is implemented by terminating the waveform when the instantaneous frequency reaches the frequency associated with the onset of the plunge or 750 Hz, whichever is lower. However, because of computational constraints, we have carried out the simulations only for high mass binaries and hence the upper cutoff plays an important role in all our simulations. It is to be noted that the discussion of the ambiguity function in Sec. III C is not valid when the upper cutoff is imposed on the waveform, though, for low mass binaries, such as NS-NS binaries, the results there are still valid. The further dependence of the signal waveform on the total mass of the system through the upper cutoff means that we can estimate the individual masses more exactly though the computational power is bound to increase.

In order to carry out the simulations for the present case we selected a $10M_{\odot}$-$1.2M_{\odot}$ binary system as this enables us to choose the filter grid well within valid limits of τ_0 and τ_1. The simulations were carried out for various values of the SNR starting from 10. The histograms of the estimated parameters at a SNR of 10 are shown in Fig. 11. At this SNR the errors obtained are $\sigma_{\tau_0} = 39.3$ ms, $\sigma_{\tau_1} = 22.4$ ms, $\sigma_{t_a} = 23.1$ ms, and $\sigma_{t_C} = 0.6$ ms. These can be compared with the values in Table II and we can see that except for the parameter t_C the errors are substantially lesser when the upper cutoff is incorporated into the waveform. It is necessary to recompute the covariance matrix, as emphasized before, including the effect of the upper cutoff in order to compare these numerically obtained values with the covariance matrix. In order to do this it is not enough to replace the upper limit in the integral in Eq. (3.19) with the upper cutoff; the waveform now depends on the total mass of the system through the upper cutoff and this information has to be incorporated into the waveform.

We carried out simulations for various SNR's for the same value of masses quoted above. In the absence of the estimates of the covariance matrix when the upper cutoff is incorporated, we assume that at a SNR of 40 the Monte Carlo estimates are consistent with those of the covariance matrix. In Fig. 12 we illustrate the results of our simulations. The dotted line is obtained through Monte Carlo estimates and the solid line is obtained by fitting a $1/\rho$ dependence of the errors on the SNR *assuming* consistency at a SNR of 40. It is seen, as in the previous simulations, that except for the parameter t_C the errors in the other parameters are fairly consistent with a $1/\rho$ dependence when $\rho > 20$.

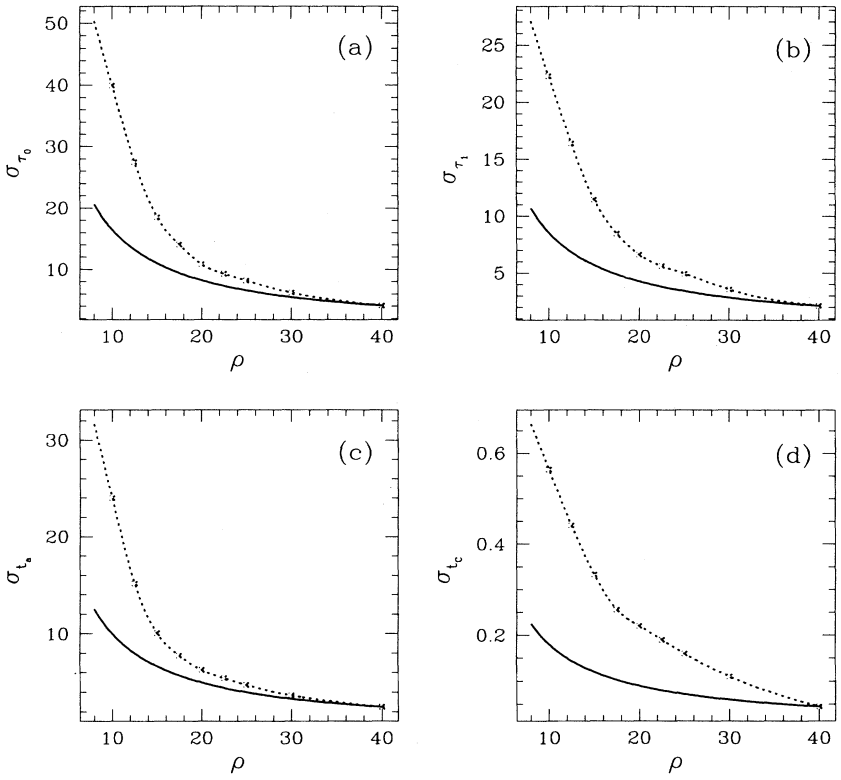

FIG. 12. The dependence of the errors on the SNR (ρ) when the upper cutoff is incorporated into the waveform.

V. CONCLUSIONS

In this paper we have explored the use of differential geometry in studying signal analysis and have addressed issues pertaining to optimal detection strategies of the chirp waveform. We have also carried out Monte Carlo simulations to check how well the covariance matrix estimates the errors in the parameters of the chirp waveform. We summarize below our main results.

(1) We have developed the concept of a signal manifold as a subset of a finite dimensional vector space of detector outputs. Using the correlation between two signal vectors as a scalar product we have induced a metric on the signal manifold. With this geometric picture it is possible to pose the question of optimal detection in a more general setting. We suggest that the set of template waveforms for the detection of the chirp signal need not correspond to any point on the chirp manifold. We propose an algorithm to choose templates off the signal manifold and show that the drop in the correlation due to the discreteness of the set of templates is reduced. This algorithm, though certainly not the best, motivates the search for more efficient templates. In addition, the chirp manifold corresponding to the second post-Newtonian waveform is shown to be effectively one dimensional. This has important implications for the computational requirement for the on-line detection of the chirp signal. The use of a convenient set of parameters of the chirp waveform for carrying out numerical and analytical simulations is stressed. These parameters are such that the metric components are independent of the parameters which implies that the manifold is flat and the corresponding "coordinate system" is Cartesian. As the metric defined is nothing but the Fisher information matrix, the covariance matrix, being the inverse of the Fisher information matrix, is also independent of the parameters.

(2) Monte Carlo simulations have been carried out for the case of the initial LIGO to find out whether the actual errors in the estimation of parameters is consistent with the values predicted by the covariance matrix. Simulations have been carried out for both the Newtonian as well as the post-Newtonian waveforms. We have restricted ourselves to the case of high mass binary systems, such as BH-NS binaries, where the computational requirement is not very heavy since the length of the data train, in such cases, works out to be less than 8 s. Nevertheless, as has been shown in this paper, the covariance matrix is independent of the parameters identified by us when waveforms are terminated at a constant upper cutoff irrespective of their masses. Consequently, our results will hold good for binary systems of arbitrary masses. We point out the major problems that arise while performing a numerical simulation and, where appropriate, we suggest how they may be taken care of. In particular, the effect of incorporating the upper cutoff in the frequency of the gravitational wave at the onset of the plunge, which essentially depends on the total mass of the binary, is extremely important for high mass binaries. Since the covariance matrix with the inclusion of such a mass-dependent upper cutoff is not available, we

have carried out most of our simulations using a constant upper cutoff. This enables us to directly compare the results of our Monte Carlo simulations with those of the analytically computed covariance matrix. Since for binaries with total mass less than $5M_\odot$ the plunge induced upper cutoff is larger than that induced by the detector noise, these effects can be ignored for such binaries.

The numerical experiments indicate that the covariance matrix underestimates the errors in the determination of the parameters even at SNR's as high as 20. In the Newtonian case the correlation coefficient of the time of arrival, t_a, and the Newtonian chirp time τ_0 is found to be very close to -1, so much so that even at a SNR of 7.5, the instant of coalescence $t_C = t_a + \tau_0$ remains practically a constant. The error in the estimation of τ_0 for the post-Newtonian waveform is about 4 times the error obtained in the case of the Newtonian waveform at the same SNR. This is expected as the first post-Newtonian correction to the waveform introduces a new parameter τ_1 (called the first post-Newtonian chirp time) which is highly (anti)correlated with τ_0. For the post-Newtonian waveform at a SNR of 10 the error in τ_0 is about 3 times that predicted by the covariance matrix. This corresponds to a factor of 2 in the chirp mass $\mathcal{M}$. The distributions for the parameters have been obtained and are seen to be unimodal distributions and are slightly more sharp than a Gaussian. When the plunge induced upper cutoff is incorporated into the waveform the errors in the estimation of parameters decrease by a factor of about 2.5. The correlation coefficient between τ_0 and τ_1 is also found to decrease, which is consistent with our discussion in Sec. IV A.

The results obtained suggest that higher moments in computing the covariance matrix may be important in the determination of the errors in parameter estimation. In the geometric picture this amounts to taking into account curvature effects, either intrinsic or extrinsic.

(3) The amplitude parameter is biased towards a higher value, as a consequence of which the distance to a coalescing binary system will be underestimated.

(4) We suggest that t_C is a more suitable parameter to estimate the direction to the source than the time of arrival. The latter is a kinematical parameter that fixes the time at which the gravitational wave frequency reaches the lower cutoff of the detector while the parameter t_C has the physical significance of being the instant of coalescence. At a SNR of 10 the error in t_a is too large (20 ms) to deduce the direction to the source accurately, whereas the error in the parameter t_C is less than 0.5 ms. This will further go down substantially for the advanced LIGO and VIRGO. A detailed analysis of coincidence detection and direction measurement is carried out in Bhawal and Dhurandhar [38] (also see [30]).

We now suggest further work which needs to be done along the lines of this paper. A full understanding of the chirp signal manifold when higher post-Newtonian corrections are incorporated into the waveform is in order. This will help in the development of more efficient algorithms for the choice of templates in the detection problem and facilitate reduction in computational time. The Monte Carlo simulations which we have carried out are for the case of a binary waveform correct up to first post-Newtonian order. Moreover, only circular orbits are considered. The effect of eccentricity is currently being investigated [39]. Performing simulations when higher post-Newtonian corrections are taken into account calls for an immense amount of computational time. Fortunately, matched filtering algorithms being amenable to parallelization [40], one could aim at using the massively parallel computers, which are now becoming available the world over, in performing such simulations.

ACKNOWLEDGMENTS

The authors would like to thank the members of the gravitational wave group at IUCAA, especially S.D. Mohanty and B. Bhawal, for many helpful discussions. R.B. was supported by the CSIR, India. We would also like to thank C. Cutler and B. Owen for their comments on an earlier version of the paper. We are also grateful to C. Cutler for sharing with us an unpublished work wherein he finds results consistent with what is reported in this study and to B. Owen for sharing his work on search algorithms prior to publication.

[1] A. Abramovici *et al.*, Science **256**, 325 (1992).
[2] C. Bradaschia *et al.*, Nucl. Instrum. Methods Phys. Res. A **289**, 518 (1990).
[3] B.F. Schutz, in *Gravitational Collapse and Relativity,* edited by H. Sato and T. Nakamura (World Scientific, Singapore, 1986), pp. 350–368.
[4] D. Marković, Phys. Rev. D **48**, 4738 (1993).
[5] L. Blanchet and B.S. Sathyaprakash, Phys. Rev. Lett. **74,** 1067 (1995).
[6] K.S. Thorne, in *Compact Stars in Binaries*, Proceedings of IAU Symposium, 1995, edited by J. van Paradijs, E. van den Heuvel, and E. Kuulkers, IAU Symposium No. 165 (Kluwer Academic, Norwell, MA, in press).
[7] K.S. Thorne, in *Proceedings of the Snowmass 95 Summer Study on Particle and Nuclear Astrophysics and Cosmology*, edited by E.W. Kolb and R. Peccei (World Scientific, Singapore, 1995).
[8] S.D. Mohanty and B.S Sathyaprakash, "A modified periodogram for the detection of gravitational waves from coalescing binaries," report, 1995 (unpublished).
[9] S. Smith, Phys. Rev. D **36**, 2901 (1987).
[10] K.S. Thorne, in *300 Years of Gravitation*, edited by S.W. Hawking and W. Israel (Cambridge University Press, Cambridge, England, 1987).
[11] C.W. Helstrom, *Statistical Theory of Signal Detection,* 2nd ed. (Pergamon Press, London, 1968).
[12] B.F. Schutz, in *The Detection of Gravitational Radiation,* edited by D. Blair (Cambridge University Press, Cambridge, England, 1989), pp. 406–427.
[13] B.S. Sathyaprakash and S.V. Dhurandhar, Phys. Rev. D **44**, 3819 (1991).
[14] S.V. Dhurandhar and B.S. Sathyaprakash, Phys. Rev. D

49, 1707 (1994).
[15] R. Balasubramanian and S.V. Dhurandhar, Phys. Rev. D **50,** 6080 (1994).
[16] K. Kokkotas, A. Krolak, and G. Tsegas, Class. Quantum Grav. **11,** 1901 (1994).
[17] T.A. Apostolatos, Phys. Rev. D **52,** 605 (1995).
[18] A. Krolak, K.D. Kokkotas, and G. Schäfer, Phys. Rev. D **52**, 2089 (1995).
[19] Shun-ichi Amari, *Differential Geometric Methods in Statistics* (Springer-Verlag, Berlin, 1990).
[20] C. Cutler and E. Flanagan, Phys. Rev. D **49**, 2658 (1994).
[21] B.J. Owen, "Search templates for gravitational waves from inspiraling binaries: Choice of template spacing," report (unpublished),
[22] L.S. Finn, Phys. Rev. D **46**, 5236 (1992).
[23] L.S. Finn and D.F. Chernoff, Phys. Rev. D **47**, 2198 (1993).
[24] L. Blanchet and B.S. Sathyaprakash, Class. Quantum Grav. **11,** 2807 (1994).
[25] A. Krolak, in *Gravitational Wave Data Analysis*, edited by B.F. Schutz (Kluwer, Dordrecht, 1989), pp. 59–69.
[26] A. Krolak, J.A. Lobo, and B.J. Meers, Phys. Rev D **48**, 3451 (1993).
[27] E. Poisson and C.M. Will, Phys. Rev. D **52**, 848 (1995).
[28] P. Jaranowski, K.D. Kokkotas, A. Krolak, and G. Tsegas, report (unpublished).
[29] B.S. Sathyaprakash, Phys. Rev. D **50**, R7111 (1994).
[30] R. Balasubramanian, B.S. Sathyaprakash, and S.V. Dhurandhar, Pramana J. Phys. (to be published).
[31] C. Cutler *et al.*, Phys. Rev. Lett. **70**, 2984 (1993).
[32] L. Blanchet, T. Damour, and B.R. Iyer, Phys. Rev. D **51**, 5360 (1995).
[33] S.V. Dhurandhar and B.F. Schutz, Phys. Rev. D **50**, 2390 (1994).
[34] William H. Press, Saul A. Teukolsky, William T. Vetterling, and Brian P. Flannery, *Numerical Recipes* (Cambridge University Press, Cambridge, England, 1993).
[35] B.J. Meers, A. Krolak, and J.A. Lobo, Phys. Rev. D **47**, 2184 (1993).
[36] L. Blanchet, T. Damour, B.R. Iyer, C.M. Will, and A.G. Wiseman, Phys. Rev. Lett. **74**, 3515 (1995).
[37] P. Jaranowski and A. Krolak, Phys Rev. D **49**, 1723 (1994).
[38] B. Bhawal and S.V. Dhurandhar (private communication).
[39] R. Balasubramanian, A. Gopakumar, B.R. Iyer, and B.S. Sathyaprakash (in preparation).
[40] B.S. Sathyaprakash and S.V. Dhurandhar, J. Comput. Phys. **109,** 215 (1993).